5-2021

Numerical Simulation of Losses in Four-Way Pipe Junctions

Simon Barth
Utah State University

NUMERICAL SIMULATION OF LOSSES IN FOUR-WAY PIPE JUNCTIONS

by

Simon Barth

A thesis submitted in partial fulfillment
of the requirements for the degree

of

MASTER OF SCIENCE

in

Civil and Environmental Engineering

Approved:

_____ Zachary B. Sharp, Ph.D., P.E. Major Professor	_____ Michael C. Johnson, Ph.D., P.E. Committee Member
_____ William J. Doucette, Ph.D. Committee Member	_____ D. Richard Cutler, Ph.D. Interim Vice Provost of Graduate Studies

UTAH STATE UNIVERSITY
Logan, Utah

2021

ABSTRACT

Numerical Simulation of Losses in Four-Way Pipe Junctions

by

Simon Barth, Master of Science

Utah State University, 2021

Major Professor: Dr. Zachary B. Sharp
Department: Civil and Environmental Engineering

This paper investigates the utility of using Computational Fluid Dynamics (CFD) for determining energy losses associated with flow passing through four-way cross junctions in pipelines. The capabilities of CFD programs have increased significantly with computing technology advances (Rodi, 2017). These technological advances make CFD a viable alternative to physical testing. However, for the best information, CFD results need to be compared to physical tests to validate them. This paper will discuss the use of CFD to reproduce physical tests performed on round-cornered four-way cross-junctions and then use the same CFD methods to produce data for sharp-cornered four-way cross-junctions.

(58 pages)

PUBLIC ABSTRACT

Numerical Simulation of Losses in Four-Way Cross Junctions

Simon Barth

To design pipelines, engineers need to know how much energy the fluid in the pipe has at different locations in the pipe network. The energy the fluid has comes in the form of pressure, velocity, and elevation. As fluid travels through a pipe, it loses energy for many different reasons. Some of those reasons include friction between the fluid and the pipe wall, shear forces within the fluid, changes in flow direction, changes in elevation, or various pipe fittings like elbows, tee's, valves, reducers, and expanders. Many of the causes of energy loss are well researched. One cause of energy loss that is not well documented is the energy loss experienced through four-way junctions in pipe networks or crosses. These junctions make the fluid lose energy differently through each of the junction's legs due to differences in flow between the legs and different changes in direction between different legs. For this paper, computer simulations were set up to determine the energy loss factor for each leg of a cross junction for various scenarios.

ACKNOWLEDGMENTS

Special thanks to Dr. Zachary Sharp for taking me on to be a part of so many projects over the years, and for the support in this research project. I would also like to thank Drs. Michael C. Johnson and Bill Doucette for agreeing to be on my committee.

I would also like to acknowledge Patrick Campana for his support in learning CFD, Shelby Bulkley for her assistance with many of the diagrams presented in this paper, and Tyler Ashby for advice and support during both undergraduate and graduate level work.

A special thanks to my friends and family for their moral support, especially to my lovely wife, Faith.

Simon Barth

CONTENTS

Page

LIST OF TABLES

Page

LIST OF FIGURES

Page

CHAPTER I

INTRODUCTION

In order to design pipelines, the amount of energy that will be lost due to friction and minor losses in pipe fittings needs to be taken into consideration. Designers have access to energy loss data for straight pipes of many different materials. Losses through pipe fittings are known for common fittings, such as elbows, tees, expansions, and reducers, but are lacking for more unique fittings like a cross. In order to find the loss coefficients for unique pipe fittings, physical data can be collected. This data can be costly and time consuming to collect due to required materials, construction, and having access to a competent laboratory for testing.

As an alternative to physical testing, Computational Fluid Dynamics (CFD) can be used to find loss coefficients. Using CFD, hydraulic information can be found for models of different geometries without having to physically test them. Computer modeling of hydraulic problems began in the 1970s, but until recent advances in computing technology, was somewhat inaccessible (Rodi, 2017). As technology advances and computing power becomes more affordable, CFD models will continue to be more complementary to physical testing.

Purpose

The purpose of this thesis is to outline a method for determining loss coefficients for four-way cross junctions using CFD. The baseline data for this project comes from previous research (Sharp, Johnson, Barfuss, & Rahmeyer, 2010) where physical data was used to determine the energy loss coefficients for a 6-inch diameter cross. Various round-edged (radius to diameter ratio of 0.33) cross flow configurations were reproduced in

CFD with turbulence models to determine which set of physics models produced loss coefficients closest to published physical data. Next, CFD was used to produce loss coefficient data for a four-way cross junction with sharp edges (no radius). Data and figures were provided so the loss coefficients for the more economical sharp-edged cross, can be used for pipeline design.

CHAPTER II

LITERATURE REVIEW

To design a pipeline, friction losses and local losses need to be known in order to adjust the geometry of the pipeline to meet the needs of the project. The effects of local losses are often negligible in long pipelines where friction loss dominates. However, in shorter systems and systems with many local losses, the effects on the flow may be significant (Tullis, 1989). In both cases, designers need coefficients to accurately predict the local losses for an adequate overall design. Loss coefficients can be provided by the manufacturer, found in textbooks, or found in previous research. Loss coefficients are available for splitting tees and bends (Miller, 1990), tees with large area ratios (Oka & Ito, 2005), tees with combining flow (Oka, Nozaki, & Ito, 1996), and expansion/contractions (Streeter & Wylie, 1975). Loss coefficients for cross junctions are limited to square edged crosses for only a few different flow combinations (Miller, 1990) and round crosses with 6-inch diameter inlet/outlet pipes and a 0.33 radius to diameter ratio (Sharp, Johnson, Barfuss, & Rahmeyer, 2010).

There have been many papers published on the use of CFD for verifying loss coefficients for different pipe fittings. In addition to studies differing in fittings tested, studies differ in chosen methods to model turbulence. Moujaes and Deshmukh (2006) determined pressure drops across round elbows and tees. Turbulence was modeled using variations on the k-ε model turbulence model and recorded as small as a 0.005 difference between K-factors and 8.1% error between CFD and observed pressure drop data. Ana Paula et al. (2014) determined losses across round elbows. Turbulence was modeled using the Realizable k-ε model and with relative error of about 10% in predicting

pressure loss. Mumma et al. (1998) determined losses in round, square, oval, and rectangular duct elbows, using the Standard k-ε turbulence model with all data falling within ±15% of physical data. Ramamurthy et al. (2006) Determined losses in rectangular duct elbows using the k-ω turbulence model with resulting CFD data that "qualitatively agrees well with the experimental flow pattern," where the dimensionless contraction coefficient determined differed by only 0.01 between physical and CFD tests.

This paper helps expands on the literature reviewed by demonstrating and determining the suitability of CFD to generate loss data for four-way crosses. Additionally, this paper expands the loss data that exists, specifically for sharp edged crosses.

CHAPTER III

EXPERIMENTAL METHODS

Theoretical Background

In a pipeline, the total energy or total head at a specific point can be determined by measuring pressure, velocity, and elevation using the expression:

$$H = \frac{p}{\gamma} + z + \frac{V^2}{2g} \tag{1}$$

where H = total head, p = pressure, γ = specific weight of fluid, z = elevation with respect to a datum, V = velocity, and g = acceleration due to gravity (32.17 ft/s).

When total head is known at two points in a system the head loss between those two points is equal to the difference in total heads as shown in the following equation:

$$\left(\frac{p_1}{\gamma} + z_1 + \frac{V_1^2}{2g}\right) - \Sigma h_L - \Sigma h_f = \left(\frac{p_2}{\gamma} + z_2 + \frac{V_2^2}{2g}\right) \tag{2}$$

where h_f = head loss due to friction and h_L = local head losses or minor head losses.

Head loss due to friction, or friction losses, comes from the fluid experiencing resistance along the pipe wall and varies depending on the roughness of the pipe material. Friction losses can be known using the following expression:

$$h_f = f\frac{L}{D}\frac{V^2}{2g} \tag{3}$$

where *f* = friction factor, *L* = length, *D* = pipe diameter. Friction factors differ between pipe materials and are easily obtained from published research, manufacturers, or experimentally (Finnemore & Franzini, 2002).

Local head loss, or local losses, can occur at expansions, contractions, junctions, turbines, valves, and other obstructions that disrupt the flow and cause turbulence. Local losses can be found using the following expression:

$$h_L = K\frac{V^2}{2g} \tag{4}$$

where K = loss coefficient. Loss coefficients differ between fitting shapes and sizes. K, the loss coefficient, is a dimensionless variable unique to different flow obstructions and varies with flow conditions such as flow velocity and pipe geometry. Like friction factors, loss coefficients need to be obtained from published research, manufacturers, or be determined experimentally (Tullis, 1989).

Loss coefficients can be determined experimentally for a junction by determining head upstream and downstream of the fitting by measuring velocities, elevations, and pressures at upstream and downstream points. This difference in head, along with accounting for friction losses allows equations 1-4 to be rearranged to solve for the loss coefficient K between Leg 1 of a junction and a downstream Leg i:

$$K = \frac{2g}{V_1^2}\left(H_1 - H_i - f\frac{L}{D}\frac{V_1^2}{2g}\right) \tag{5}$$

Depending on flow configuration, the loss coefficient can be either negative or positive, regardless they will be referred to as loss coefficients throughout this paper.

One method for determining the needed hydraulic information to determine loss coefficients is through the use of CFD. While the concepts behind CFD have existed for decades, major progress in the field is accelerating rapidly alongside progressing computing technology (Rodi, 2017). This is due to the computational power often needed to use CFD applications accurately. CFD works by discretizing a desired hydraulic

system into cells in a grid and solving governing equations for each discrete cell. These computational grids or meshes often have very small individual cells in large numbers to fully define flow phenomena and therefore require significant computational resources. CFD can be used to find solutions to hydraulics problems without having to physically construct models or prototypes to perform physical tests. CFD models can simplify the process of fine-tuning designs by allowing changes to be made to a computer model before any physical prototype is constructed (Andersson, et al., 2011).

The governing equations at the root of most CFD methods are the Navier-Stokes equations. The Navier-Stokes Equations solve continuity and momentum for fluid flow in three dimensions (Cebeci, Kafyeke, & Laurendeau, 2005). Solving the Navier-Stokes Equations is called Direct Numerical Simulation (DNS). Theoretically, DNS is the most accurate way to simulate a flow. However, for turbulent flows the grid must be as fine as the smallest eddies which would be computationally impractical for most problems. Because of this, DNS is limited to solving laminar flows or small models (Durbin & Petterson Reif, 2011).

To reduce the computational power needed to resolve the flows in a model, the Navier-Stokes Equations can be Reynolds averaged. Reynolds Averaged Navier-Stokes equations (RANS) remove fluctuations from variables in the flow field (Kajishima & Taira, 2017). With RANS, the effects of turbulence on the flow are considered by including a term called eddy viscosity.

Turbulence models are used to allow CFD simulations to replicate the effects of turbulence without requiring a mesh fine enough to simulate all vortices and eddies. Turbulence models statistically solve for eddy viscosity on the flow field instead of

explicitly simulating the countless micro-eddies that occur through the flow. Many turbulence models have been studied and used. Commonly used turbulence models include the k-ε model, the k- ω model, Large Eddy Simulation (LES), and Detached Eddy Simulation (DES). There are many other turbulence models and variations of each model. The many models and variations have been created because there is no single turbulence model that is applicable to all types of flow. (Kajishima & Taira, 2017).

The k-ε model is the most widely used turbulence model (Rodi, 2017). The standard k-ε Model is a two-equation RANS-based model for solving turbulent transport. The k-ε model employs a turbulent energy equation to solve for k and an energy dissipation equation to solve for ε. The variables k and ε are dimensionless values used to predict the eddy viscosity (Jones & Launder, 1973). The benefits of using the k-ε model are it is well known and well researched and gives reliable results (Durbin & Petterson Reif, 2011). Even though some do not recommend this model in cases of complicated flows, including curved boundary layers and mixing flows (Larsson, Lindmark, Lundstrom, & Nathan, 2011) it is still considered the industry "work horse" providing reliable solutions for many types of problems.

The k-ω model is similar to the k-ε model. The variable k and ω are determined to solve for eddy viscosity. The variable k and ω are dimensionless variables that represent turbulent energy and dissipation, respectively. The k-ω model is used as much as the k-ε model (Kajishima & Taira, 2017).

Large Eddy Simulation (LES) began being developed in 1970. LES allows a coarser grid than DNS by resolving only large eddies, and numerically modeling the effect of eddies smaller than the grid. Eddies smaller than the grid are modeled through a

sub-grid scale model. By having a coarser grid, flows can be resolved with less computational power than DNS for complex flows and flows with high Reynolds numbers. However, LES is much more computationally expensive than other turbulence models (Rodi, 2017) and is only practical to use in low Reynolds number applications.

Detached Eddy Simulation (DES) is a modeling approach that combines aspects of LES and RANS simulations. Boundary layers and simple flows are solved with the RANS equations, while the turbulent flows are solved with LES and a sub-grid scale model (Rodi, 2017).

Four-Way Cross Junctions

Because cross junctions have four openings, there are four different flow configurations possible. Configurations include dividing flow (one inlet, three outlets), combining flow (three inlets, one outlet), perpendicular flow (two perpendicular inlets, two perpendicular outlets), and colliding flow (two opposing inlets, two opposing outlets) as shown in Figure 1. Throughout the paper, flow legs will be numbered 1-4 clockwise, starting at the left leg, as shown in Figure 1.

Experimental Setup

A physical study was previously performed at the Utah Water Research Laboratory (UWRL) to find the loss coefficients for four-way crosses with round radius corners (Sharp, Johnson, Barfuss, & Rahmeyer, 2010). For the physical study, a steel four-way cross was used to run different flow configurations to be able to provide a comprehensive list of coefficients. The physical study was replicated in CFD to determine which turbulence model best simulates four-way cross junction flow before attempting to produce loss coefficient data for sharp-edged cross-junctions.

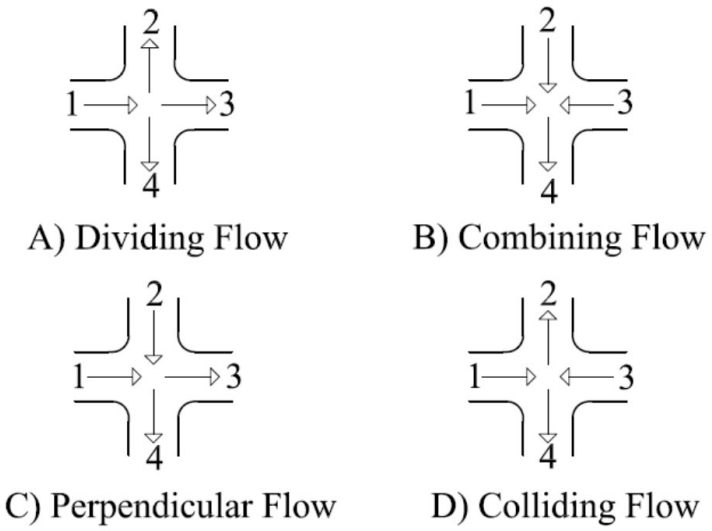

Figure 1. Four-way cross-junction flow configurations (Sharp, Johnson, Barfuss, & Rahmeyer, 2010).

Geometry

To best replicate the physical study, the dimensions of the physical study's junction were measured and reproduced in the computer model to reduce error due to geometrical differences. The inside diameters were found, and flaws such as offset joints and tapered edges were replicated in the computer model's geometry (Figure 2).

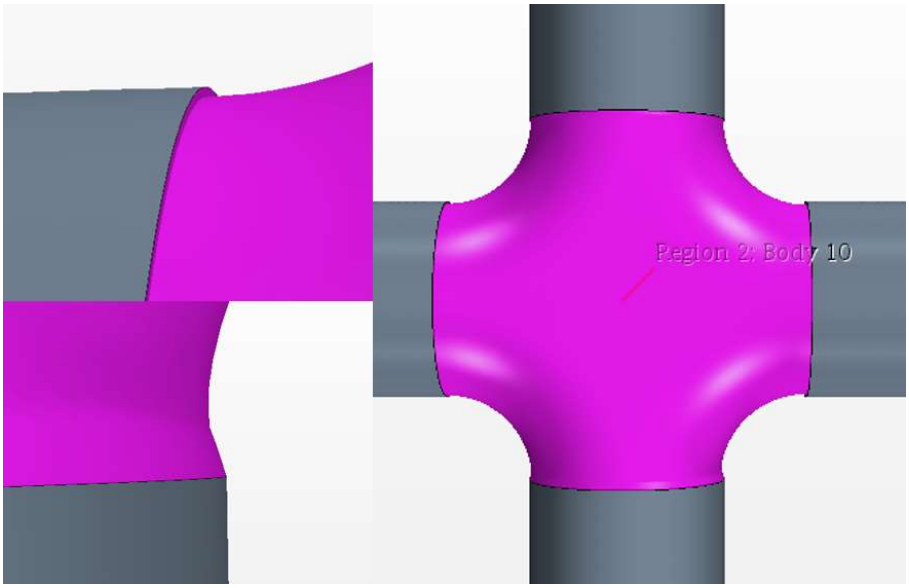

Figure 2. CAD Drawing of round-cornered cross with tapered and offset edges.

Meshing

The model was split into grid cells using meshing models built into STAR-CCM+. Meshing models used were the polyhedral mesher, the prism layer mesher, and a surface remesher. The polyhedral mesher is a volume mesher that draws a grid throughout the volume of the model with polygonal cells rather than cuboid or tetrahedral cells. A polyhedral mesh can create a grid with fewer cells than with other cell shapes (Siemens, 2020). The prism layer mesher is a subsurface mesher that controls the cells drawn near boundaries. The prism layer cells are better suited to accurately simulate the friction that fluid experiences near a boundary. The surface remesher creates a mesh that represents the boundary of the model. The surface remesher improves the surface for the volume mesher and the subsurface mesher (Siemens, 2020). Figure 3 shows a mesh labeled to illustrate a generic volume mesh and surface mesh, in contrast to mesh used in this research.

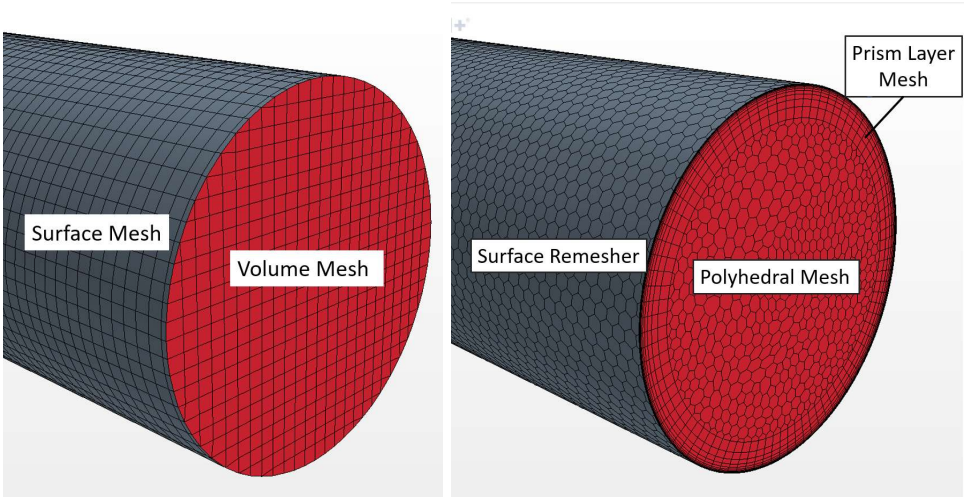

Figure 3. Example of volume mesh and surface mesh with a generic grid (left). Mesh generated using polyhedral mesher, surface remesher, and prism layer meshers (right).

In order to decrease the computing time, a coarse base cell size was chosen to mesh the entire model, and volumetric controls and parts-based meshes were used to apply finer meshes to areas with higher local velocities and local turbulence. Volumetric controls and parts-based meshing allow the user to select sections of the model to receive specific meshing conditions, such as different cell sizes or different meshing models. 36 inches along each leg of the model were set to have mesh cells 80% the size of the base mesh size and the cross-junction cells were set to be 70% the size of the base mesh size. Finer mesh in high turbulence areas improves the accuracy of the model (Durbin & Petterson Reif, 2011).

Uncertainty

The numerical uncertainty associated with the solution due to discretization error can be reduced by changing the size of the grid cells of the mesh in a model. Once the grid cells are small enough, simulation results become independent of cell size (Celik, et al., 2008). Once results are independent of the grid, grid cell size reduction is unnecessary and increases computational power needed to resolve the grid. ASME provides a procedure for determining uncertainty due to discretization by determining when the model results become independent of the mesh (Celik, et al., 2008). The base sizes used for the estimation of discretization error were 0.18, 0.25, and 0.35 inches. Celik, et al. says to report the apparent order (p), the approximate relative error (e^{21}_{a}), the extrapolated relative error (e^{21}_{ext}), and the fine-grid convergence index (GCI^{21}_{fine}). Because each simulation produces three coefficients, there are three of every reported value (Table 1). Because all simulations are similar, one grid convergence test was performed. With a maximum value GCI^{21}_{fine} of 0.61 out of the three legs, solution was shown to be

independent of the grid for the 0.25-inch base cell size.

Table 1. Grid convergence discretization error values.

	K 1-2	K 1-3	K 1-4
p	16.50	8.21	9.82
e^{21}_a	1.52%	6.78%	3.53%
e^{21}_{ext}	0.01%	0.49%	0.15%
GCI^{21}_{fine}	0.01%	0.61%	0.18%

CFD Physics

The physics settings in STAR-CCM+ were set to model constant density water at 60 °F (by setting the density to 62.36629 lb/ft^3 and dynamic viscosity to 1.12193 cP). The model was set to simulate steady, three-dimensional, turbulent flow. Initially, the default settings were used for a turbulence model (Realizable K-Epsilon Two-Layer), but the model used to determine the final data was the Standard K-Epsilon Two-Layer.

CFD Friction

In order to determine the net K-factors the friction of the pipe needs to be known. This is the case for physical and numerical data. To determine the friction factor of the CFD model, a straight pipe was modeled and flows of different velocities were passed through it until equilibrium was reached. Because the wall boundary conditions are a no slip boundary the wall velocity becomes zero in the numerical model and friction loss occurs. Flow rate, fluid properties, and geometry of the pipe were used to determine the friction factor using equation 3. The Reynold's number (*Re*) was then determined for each flow velocity tested and a relationship between *Re* and *f* was found (Figure 4).

Reynolds number is determined by the following expression:

$$Re = \frac{V*D}{v} \quad (6)$$

Where Re = Reynolds number, and v = kinematic viscosity (Finnemore & Franzini, 2002).

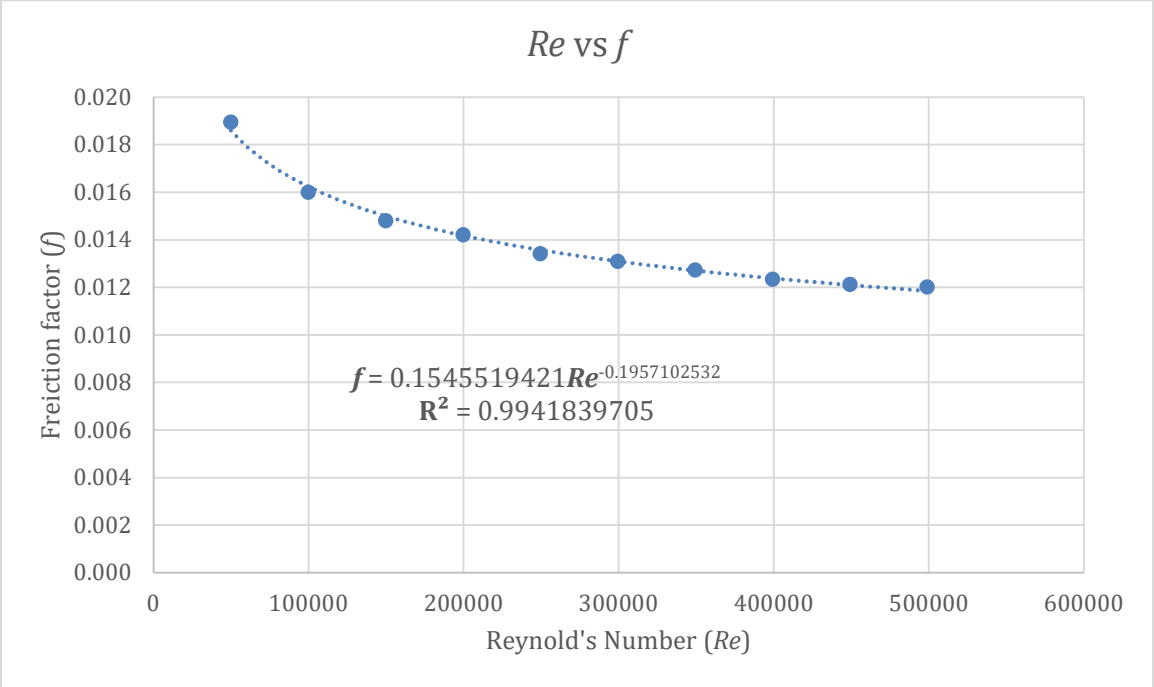

Figure 4. Relationship between Reynolds number and CFD model friction factor.

Boundary Conditions

Flow rates for inlets were defined by inputting a mass flow rate at the inlet boundary. Flow rates for outlets were defined by determining a what fraction of the flow exits through a specific leg. The outlet boundary was assigned a flow split ratio.

CFD Output Data

The information gathered from the CFD model are taken from each leg 36 inches from the junction at same location as the pressure taps during the physical test. The

values obtained from the CFD model were velocity, cross sectional area, and pressure.

The velocity was taken from a plane 36 inches from the junction along each leg. Velocities were only measured in the direction orthogonal to the measurement plane. When a velocity magnitude is used, inaccurate measurements are recorded due to lateral flows from swirling or turbulence. Velocities recorded show a positive (+) sign for flows into the model and a negative (-) sign for flows leaving the model.

Cross-sectional areas were taken from a plane perpendicular to the flow. An area report from the mesh was used rather than of solving for the area based on the modeled diameter. Using the meshed area is more accurate than determining area based on the input geometry, due to the slight changes in geometry that occur during meshing. The cross-sectional area was used to determine pipe diameter for use in equations 1-5.

The pressure was measured on the same plane at four points on the pipe wall at locations 45°, 135°, 225°, and 315° clockwise from the top of the pipe. The average of the four pressures was recorded. The pressure was measured in the CFD model after this manner to replicate the physical model, which measured pressure at four pressure taps at the same locations.

Twelve preliminary simulations were run matching physical runs to determine how well CFD replicates UWRL physical test. A summary of the 12 comparison runs are shown in Table 2 using the default Realizable k-ε turbulence model. The CFD determined loss coefficients, *K*, that showed the most difference from the physical data were losses between high and low flow inlets and outlets. In most cases the magnitude of the coefficients between the physical and CFD coefficients are similar. The sign (positive or negative magnitude) of the coefficients are the same between the physical and CFD

data, except in four cases. The four coefficients with conflicting signs have magnitudes of 0.25 or smaller. K factors of this magnitude could be considered negligible in many applications.

The coefficients' magnitudes range from as small as 0.03 to as large as 81.6. The data with the biggest differences between the physical and CFD coefficients are relatively large values for loss coefficients. These large coefficients with significant differences all occur between high velocity legs and low velocity legs. This may indicate that loss coefficients determined using these methods used are increasingly less accurate as the flow leg of interest approaches zero flow. It should be noted that to determine the head loss that occurs in a near zero velocity leg, the velocity in that leg is used, and smaller velocities produce smaller absolute head losses making the head loss in these legs less critical to a system.

Turbulence Model

In addition to the twelve runs, six runs were performed with different turbulence models. The turbulence models that were tested were the k-ε, k-ω, LES, and DES. There are several variations of the k-ε model that have been developed to better suit different situations. Some of the k-ε models that the STAR-CCM+ Manual recommends for turbulent models include the Standard, Realizable, Elliptic Blending, and V2F k-ε models. Each of these models was run for the same flow configuration and compared to the physical results to determine which model produces the loss coefficient. The loss coefficients produced by each model for each leg are shown in Figures 5-7. The flow configuration for each of the six turbulence model simulations had 80% of the inflow through Leg 1, 20% of the inflow through Leg 2, 20% of the outflow through Leg 3, and

80% of the outflow through Leg 4. The turbulence models that replicated the physical data best were the standard k-ε model and the realizable k-ε model (Figures 5-7). The standard k-ε model produced a loss coefficient closer to the physical data than the realizable for two of the three coefficients. The realizable k-ε model was closer to the physical data than the normal for the third coefficient.

Because the results between the realizable and standard k-ε models were so close, the same twelve simulations that were originally run with the realizable k-ε model were run again with the standard k-ε model to determine which model to use for the sharp-edged runs. The standard k-ε model simulations are shown in Table 3. The results confirmed that the standard k-ε model consistently produces loss coefficients closer to the physical data.

Table 2. Comparison of K Factors between CFD with Realizable k-ε turbulence model and physical test data.

	Qn/Qt				CFD K Factor (Realizable k-ε)			Physical K Factor			Magnitude Difference		
Run	Leg 1	Leg 2	Leg 3	Leg 4	K_{1-2}	K_{1-3}	K_{1-4}	K_{1-2}	K_{1-3}	K_{1-4}	K_{1-2}	K_{1-3}	K_{1-4}
P1	1	-0.3	-0.3	-0.3	5.73	-0.30	5.80	5.53	0.07	6.20	0.20	-0.37	-0.40
P2	1	-0.3	-0.1	-0.6	6.63	1.85	1.63	8.89	12.29	2.43	-2.26	-10.44	-0.80
P3	1	-0.3	-0.6	-0.1	8.63	0.09	81.58	6.81	-0.06	66.81	1.82	0.15	14.77
P4	0.5	0.5	-0.5	-0.5	0.04	0.56	0.56	-0.03	0.35	0.40	0.07	0.21	0.16
P5	0.8	0.2	-0.2	-0.8	10.98	10.42	0.68	9.34	8.84	0.48	1.64	1.58	0.20
P6	0.8	0.2	-0.5	-0.5	12.37	1.32	1.88	10.53	1.03	1.37	1.84	0.29	0.51
P7	0.5	-0.5	0.5	-0.5	2.96	-0.09	2.94	1.20	-0.01	1.19	1.76	-0.08	1.75
P8	0.9	-0.9	0.1	-0.1	0.63	44.22	55.75	0.77	27.29	60.89	-0.14	16.93	-5.14
P9	0.8	-0.5	0.2	-0.5	1.40	-0.61	1.41	2.31	-0.01	2.25	-0.91	-0.60	-0.84
P10	0.3	0.3	0.3	-1	-0.35	-0.07	0.15	-0.44	-0.03	0.04	0.09	-0.04	0.11
P11	0.2	0.6	0.2	-1	-0.87	-0.11	-0.03	-0.85	-0.18	-0.15	-0.02	0.07	0.12
P12	0.2	0.4	0.4	-1	-0.84	-0.64	0.07	-0.88	-0.58	-0.04	0.04	-0.06	0.11

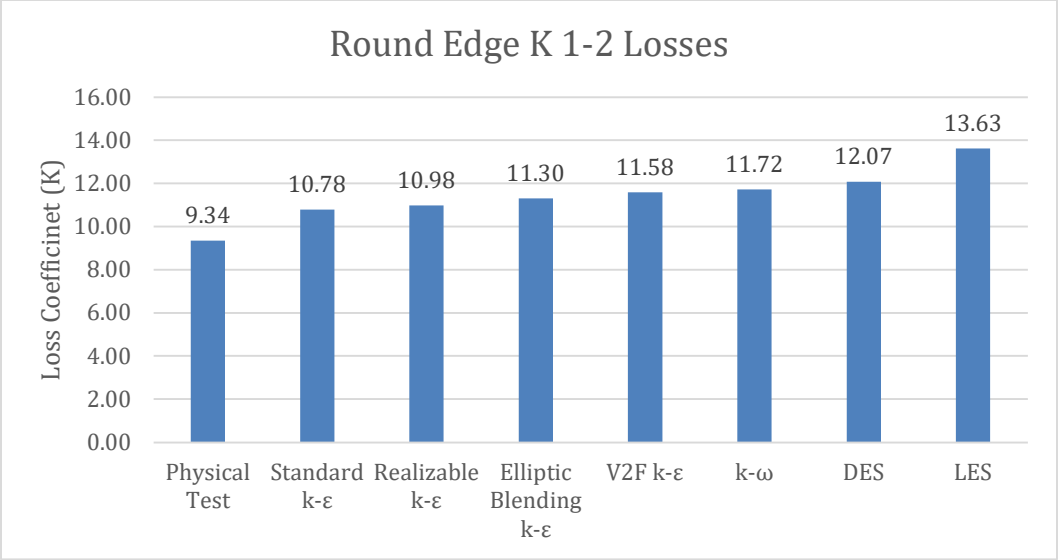

Figure 5. Loss coefficients between leg 1 and 2 using different turbulence models.

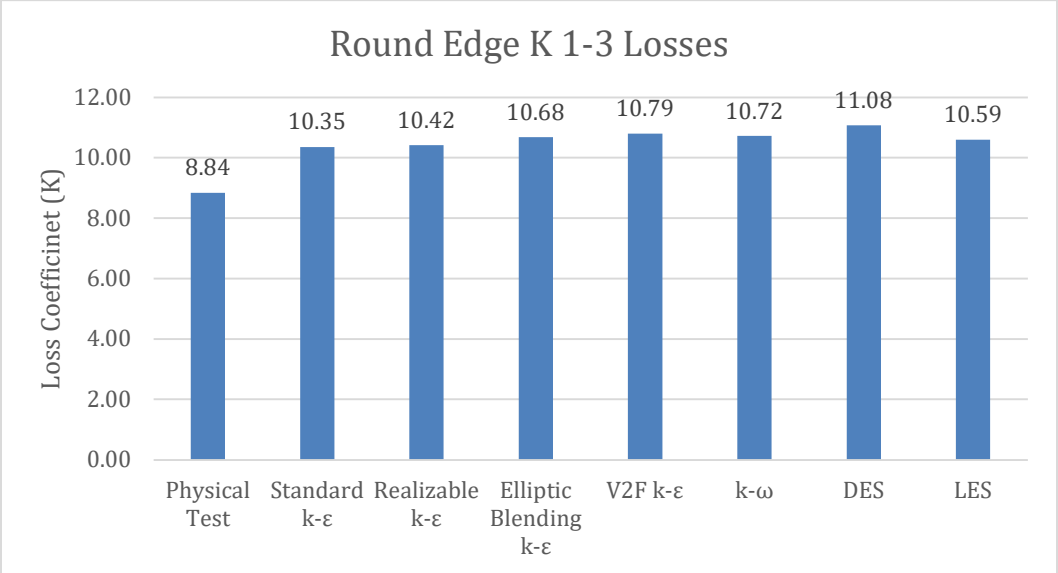

Figure 6. Loss coefficients between leg 1 and 3 using different models.

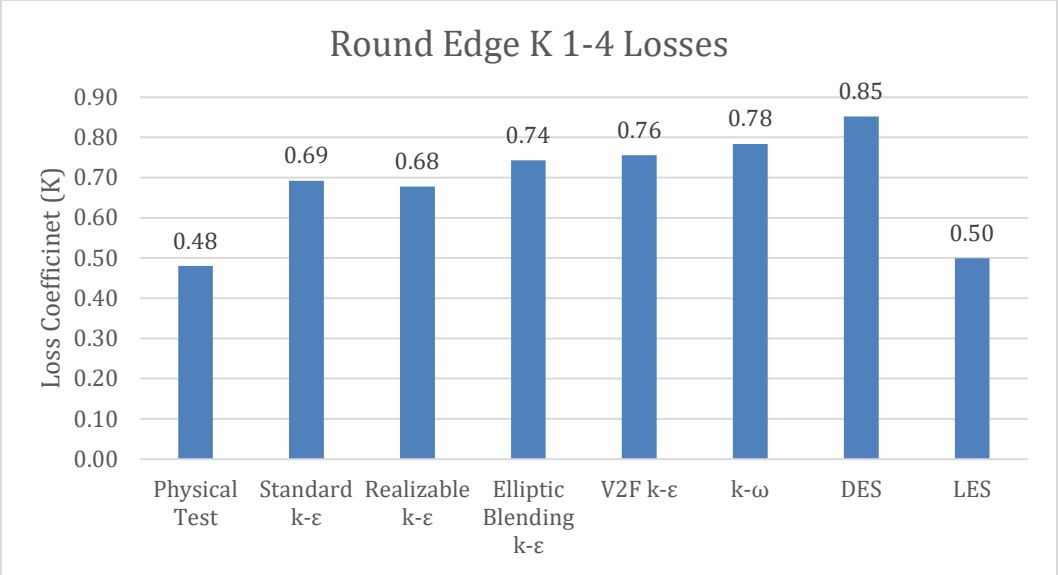

Figure 7. Loss coefficients between leg 1 and 4 using different models.

Table 3. Comparison of K Factors between CFD with Standard k-ε Turbulence model and Physical test data.

	Qn/Qt				CFD K Factor (Standard k-ε)			Physical K Factor			Magnitude Difference		
Run	Leg 1	Leg 2	Leg 3	Leg 4	K_{1-2}	K_{1-3}	K_{1-4}	K_{1-2}	K_{1-3}	K_{1-4}	K_{1-2}	K_{1-3}	K_{1-4}
P1	1	-0.3	-0.3	-0.3	5.56	-0.08	5.62	5.53	0.07	6.2	0.03	-0.15	-0.58
P2	1	-0.3	-0.1	-0.6	6.75	4.83	1.62	8.89	12.29	2.43	-2.14	-7.46	-0.81
P3	1	-0.3	-0.6	-0.1	8.17	0.14	78.86	6.81	-0.06	66.81	1.36	0.20	12.05
P4	0.5	0.5	-0.5	-0.5	0.05	0.54	0.52	-0.03	0.35	0.4	0.08	0.19	0.12
P5	0.8	0.2	-0.2	-0.8	10.78	10.35	0.69	9.34	8.84	0.48	1.44	1.51	0.21
P6	0.8	0.2	-0.5	-0.5	12.03	1.34	1.76	10.53	1.03	1.37	1.50	0.31	0.39
P7	0.5	-0.5	0.5	-0.5	0.95	-0.01	0.98	1.2	-0.01	1.19	-0.25	0.00	-0.21
P8	0.9	-0.9	0.1	-0.1	0.69	41.01	54.37	0.77	27.29	60.89	-0.08	13.72	-6.52
P9	0.8	-0.5	0.2	-0.5	2.07	1.69	2.10	2.31	-0.01	2.25	-0.24	1.70	-0.15
P10	0.3	0.3	0.3	-1	-0.33	-0.07	0.19	-0.44	-0.03	0.04	0.11	-0.04	0.15
P11	0.2	0.6	0.2	-1	-0.84	-0.11	0.00	-0.85	-0.18	-0.15	0.01	0.07	0.15
P12	0.2	0.4	0.4	-1	-0.81	-0.64	0.11	-0.88	-0.58	-0.04	0.07	-0.06	0.15

Experimental Procedure

Using what was learned from the round-edged model simulations, sharp edged simulations were set up. A new geometry was created to represent a sharp-edged cross. Each sharp-edged simulation used the same physics and meshing models. The selected turbulence model was applied. 99 Simulations were set up to represent 215 different cases with different flow configurations and flow ratios.

A three-dimensional model was made for a 6-inch 90° cross junction. Like the round-cornered model, measurements were taken on a plane 36 inches upstream/downstream of inlet/outlet legs (Figure 8). A length of 10-diameters (60 inches) of straight pipe lead up to each of the measurement planes to minimize the affect inlet or outlet boundaries affect the flow.

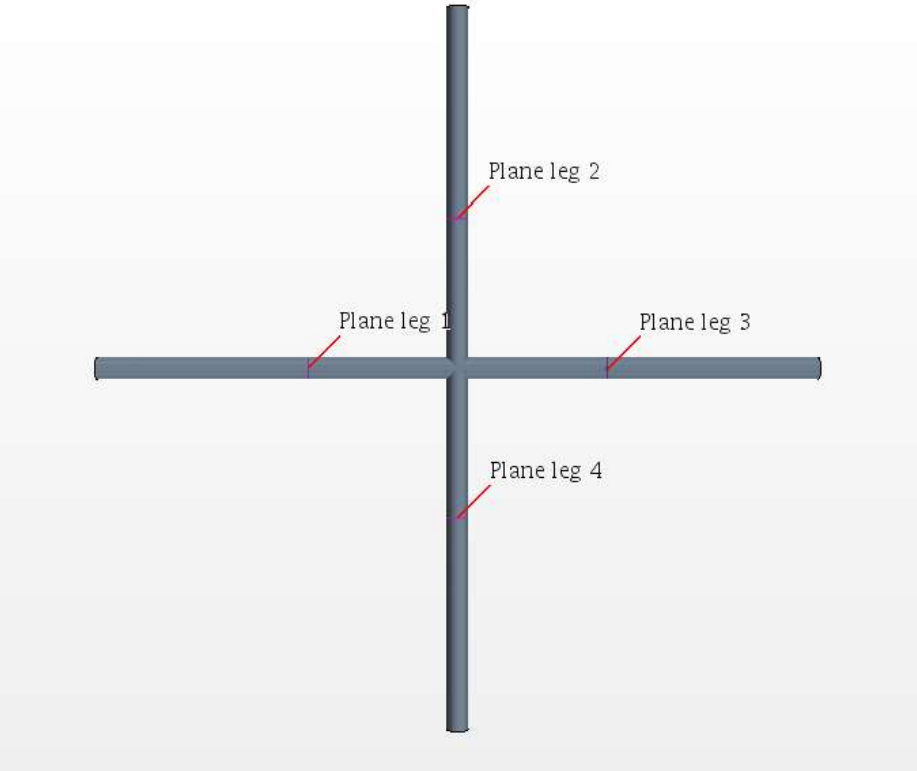

Figure 8. Four-way sharp-cornered 90° cross junction and measurement planes.

Velocity, pressure, and area were recorded in each leg for each simulation and equations 1-5 were used to determine the loss coefficients between Leg 1 to Legs 2-4. Velocity and area were measured following the same method as for the round edged preliminary model. As mentioned previously, velocities recorded show a positive (+) sign for inflows and a negative (-) sign for outflows. The friction factor was determined using the same line fit as the round edged model (Figure 4). The pressure was taken at four points near the wall on the same plane, 36 inches from the junction in each leg. The four points were 45°, 135°, 225°, and 315° clockwise from the top of the pipe.

Simulations

Symmetrical simulations were not performed, but data was mirrored for computational efficiency. Simulation flow configurations and split ratios and loss coefficients for the sharp-cornered model are found in Appendix A. Contour diagrams were produced to allow for loss values between explicitly modeled flows to be determined (Nikfetrat, Johnson, & Sharp, 2015).

CHAPTER IV

RESULTS AND DISCUSSION

Data

The results of the simulations are shown in tabular form in Appendix A. In order to predict flow configurations not explicitly modeled, three contour diagrams were produced for each flow configuration. The loss coefficients are represented by the values shown on the contours. Inflows and outflows are all described as positive ratios for the plots, and flow directions are illustrated by arrows on each plot for clarity.

For all cases where zero flow is present, the losses between the inlet and the zero-flow leg is undefined. As the flow in a leg decreases, approaching zero, the loss coefficient increases until it is considered an undefined value. Undefined values are represented by infinity in Appendix A.

The dividing and combining flow configurations were plotted on ternary diagrams. The dividing flow losses are shown in Figures 9-11. For the dividing flow ternary diagrams, axes represent the flow ratios of the outflows in legs 2-4 to the total flow in leg 4. The combining flow losses are shown in Figures 12-14. For the combining flow ternary diagrams, axes represent the flow ratios of the inflows in legs 1-3 to the total flow in the system.

The perpendicular and colliding flow configurations were plotted on four-axis diagrams. For the perpendicular flow diagrams, axes represent flow ratios of all legs to total flow, as labeled in Figures 15-17. For the colliding flow diagrams, axes represent flow ratios of all legs to total flow, as labeled in Figures 18-20.

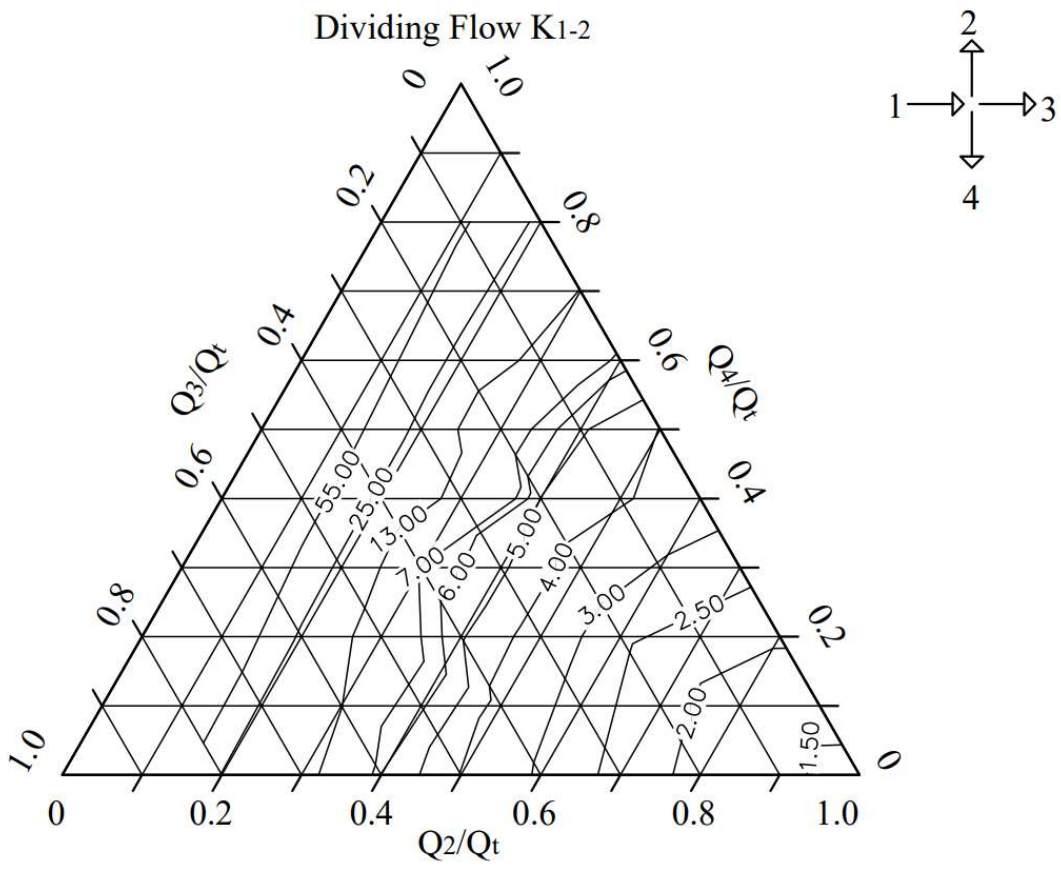

Figure 9. Loss coefficients for Dividing Flow between Leg 1 and 2.

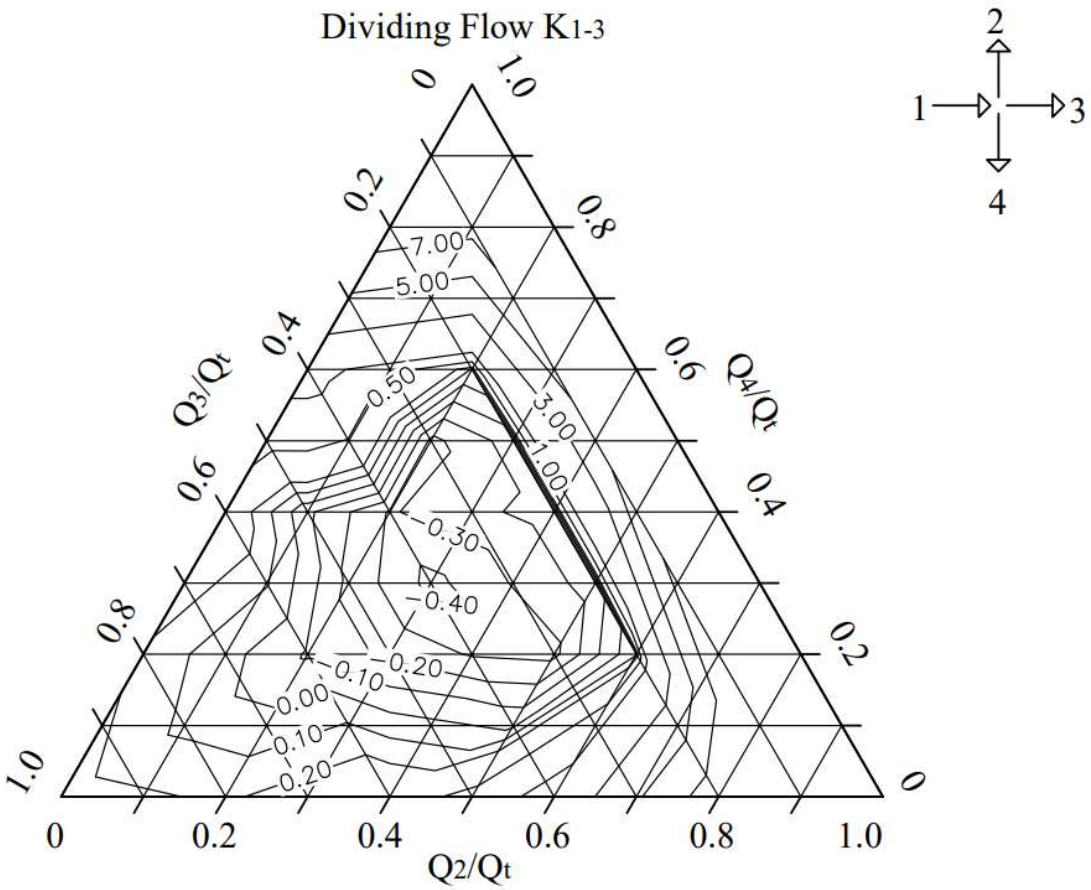

Figure 10. Loss coefficients for Dividing Flow between Leg 1 and 3.

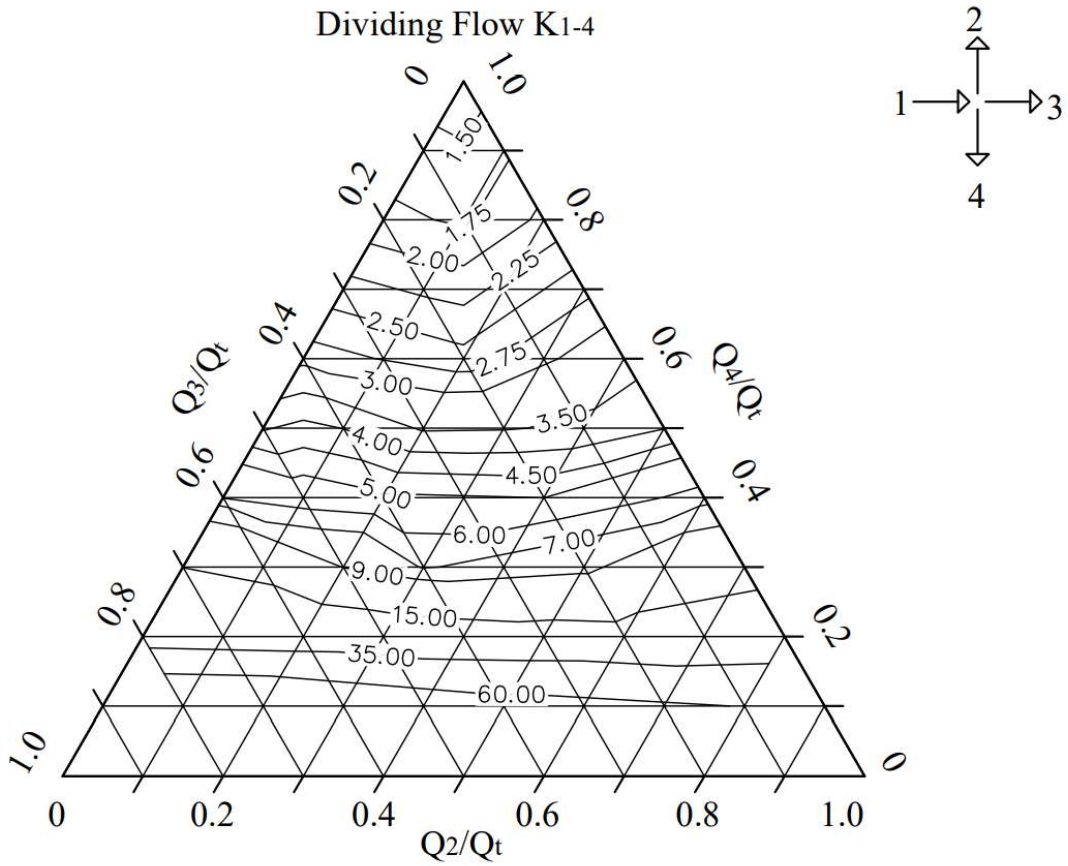

Figure 11. Loss coefficients for Dividing Flow between Leg 1 and 4.

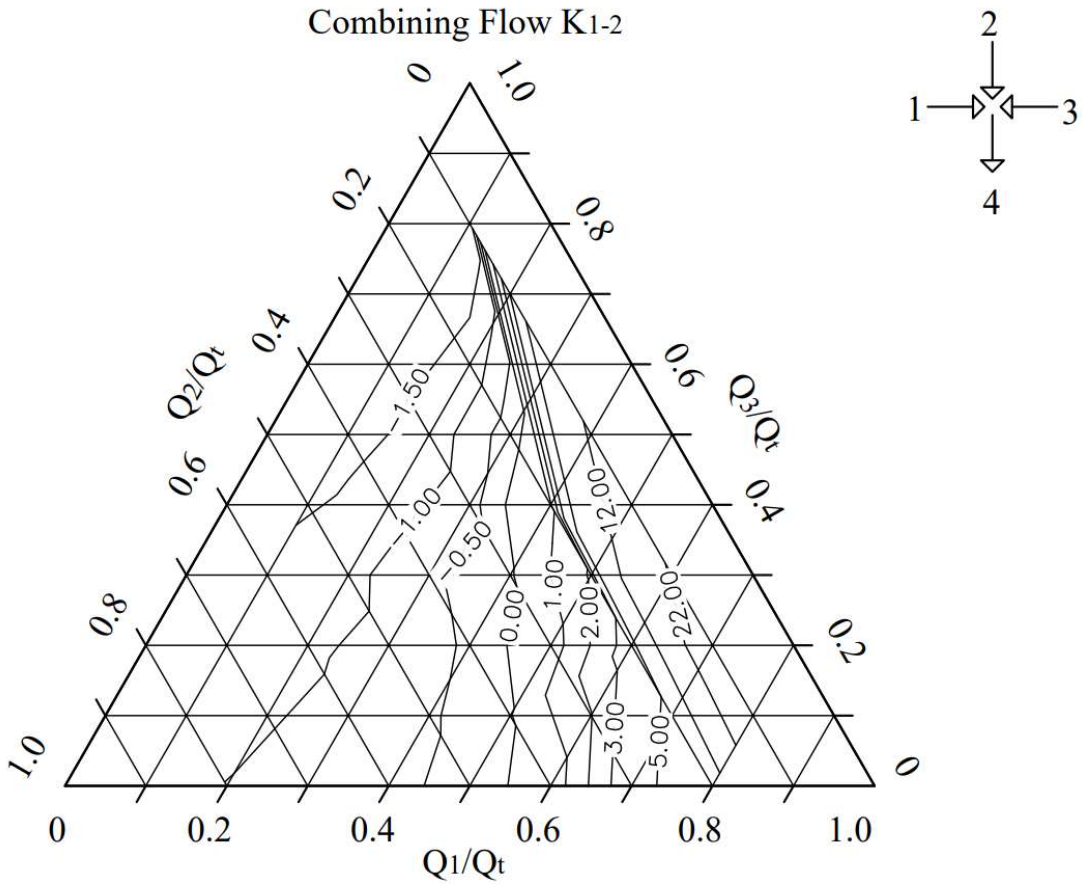

Figure 12. Loss coefficients for Combining Flow between Leg 1 and 2.

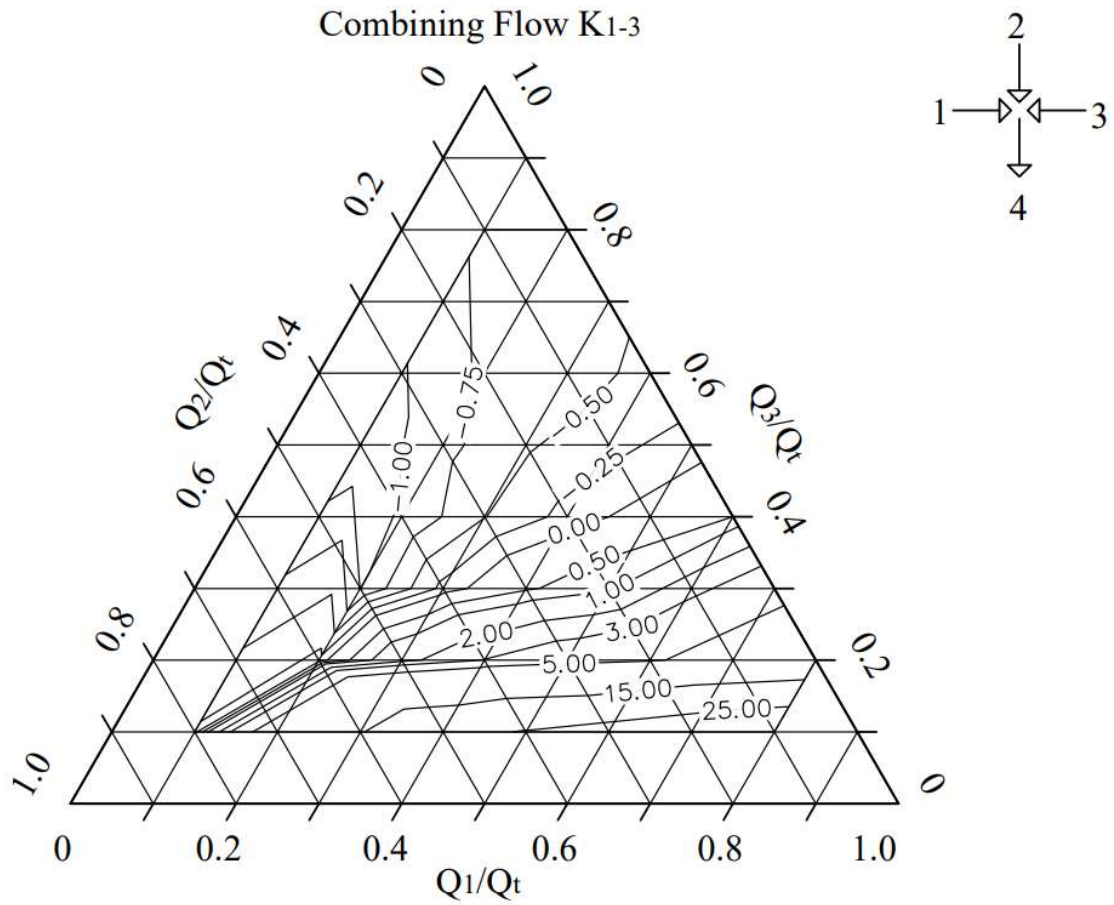

Figure 13. Loss coefficients for Combining Flow between Leg 1 and 3.

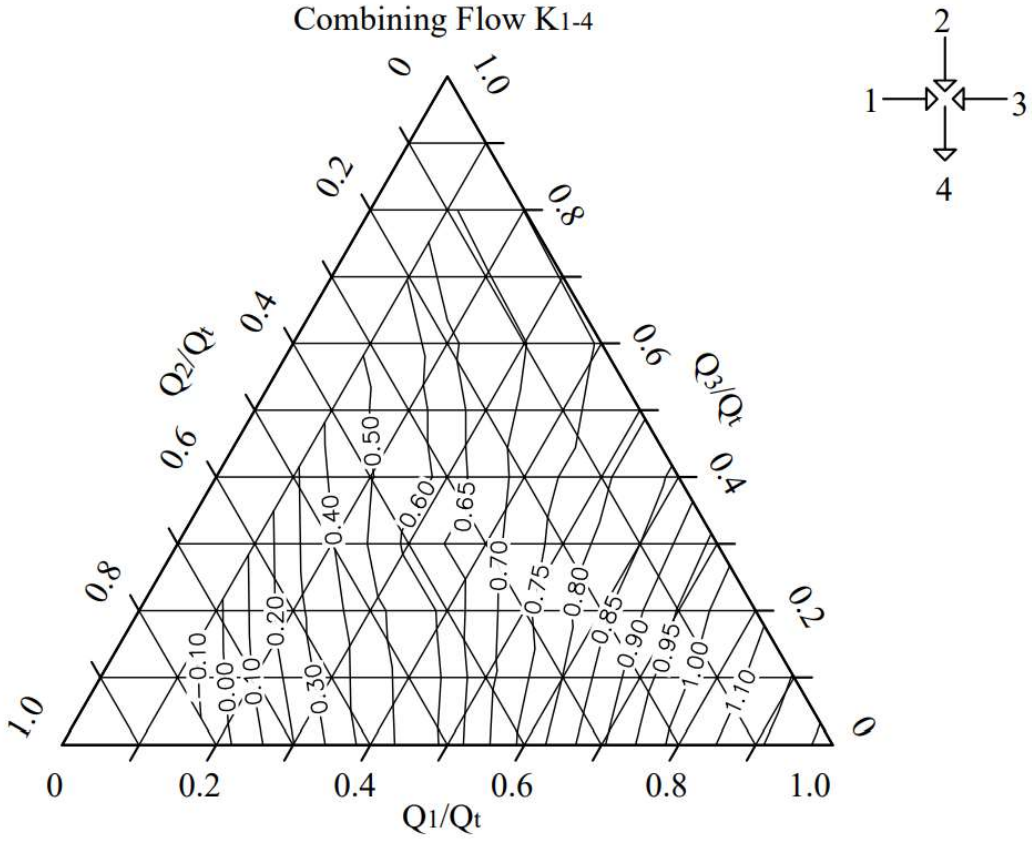

Figure 14. Loss coefficients for Combining Flow between Leg 1 and 4.

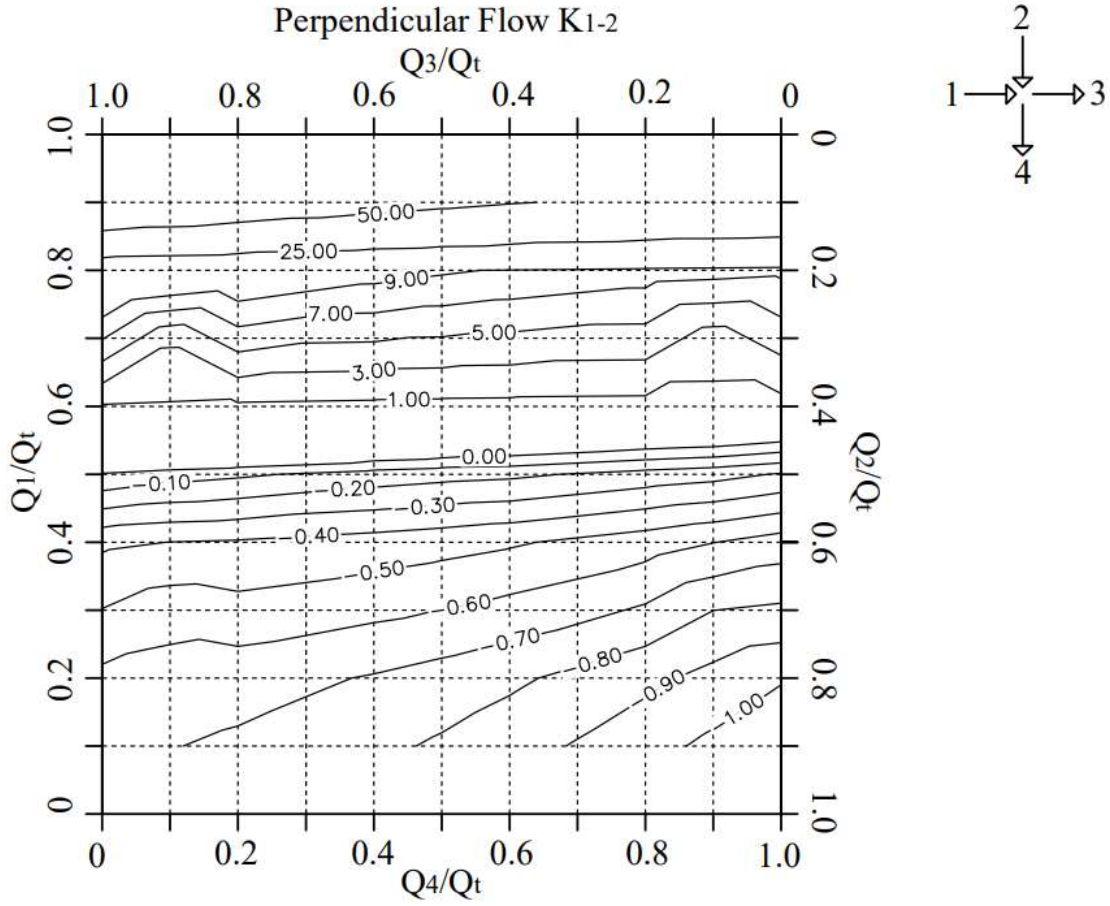

Figure 15. Loss coefficients for Perpendicular Flow between Leg 1 and 2.

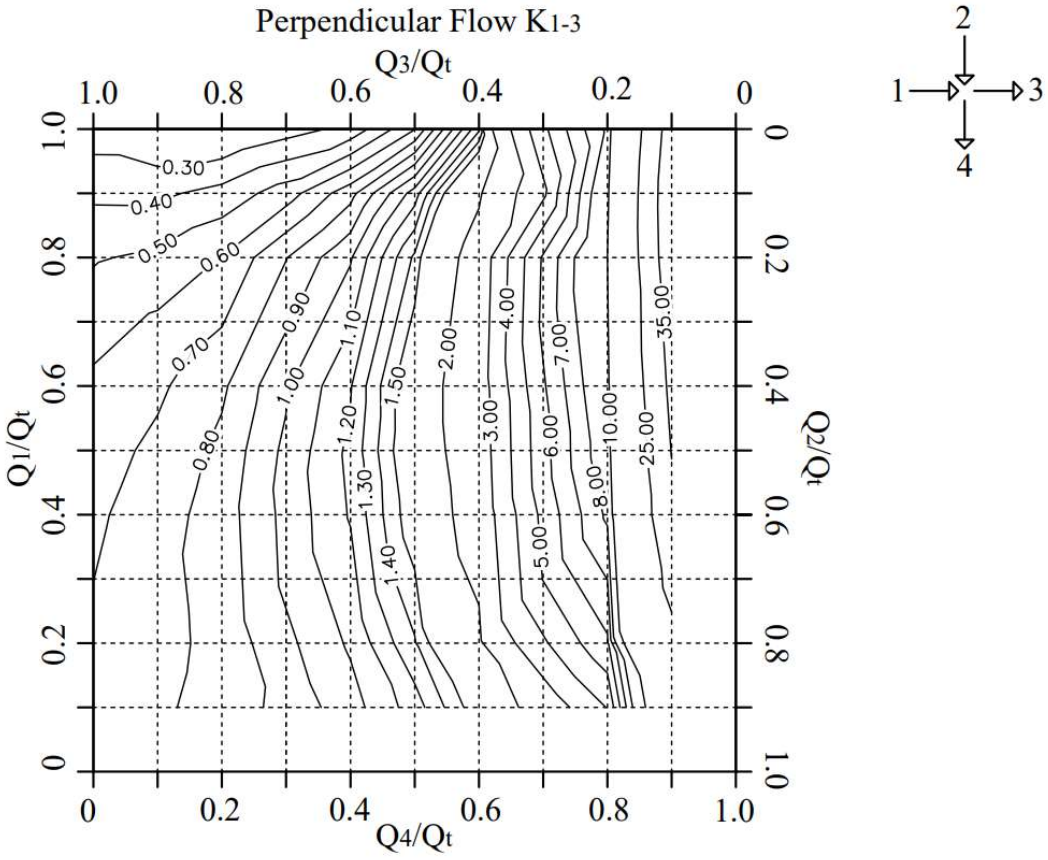

Figure 16. Loss coefficients for Perpendicular Flow between Leg 1 and 3.

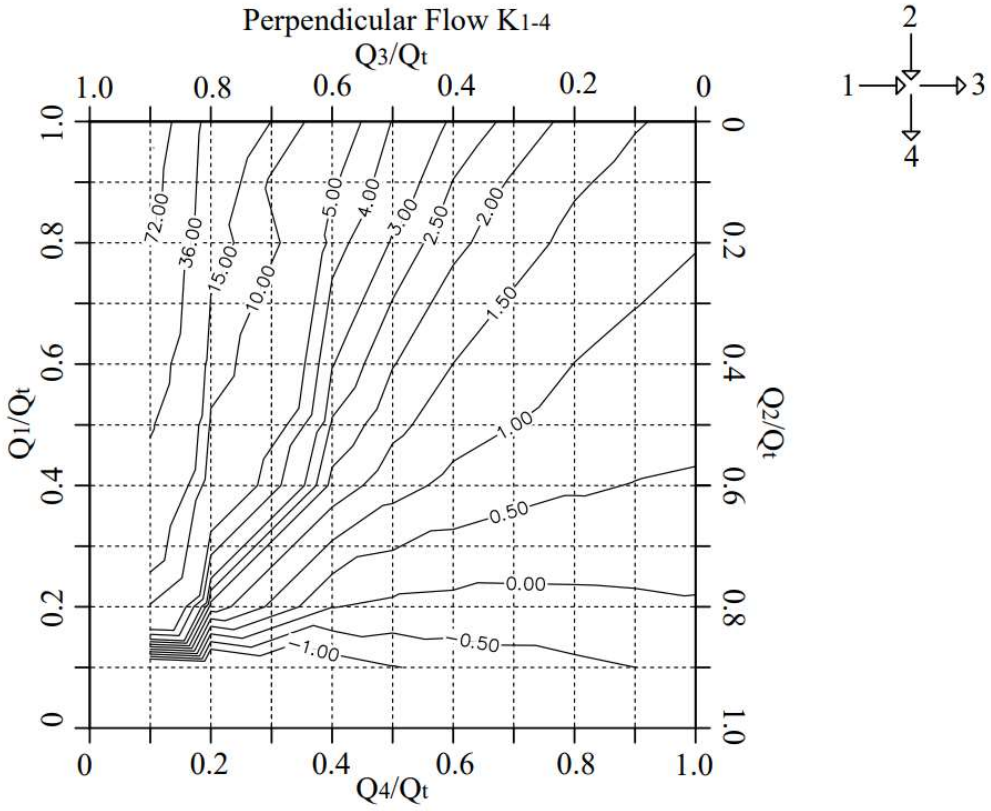

Figure 17. Loss coefficients for Perpendicular Flow between Leg 1 and 4.

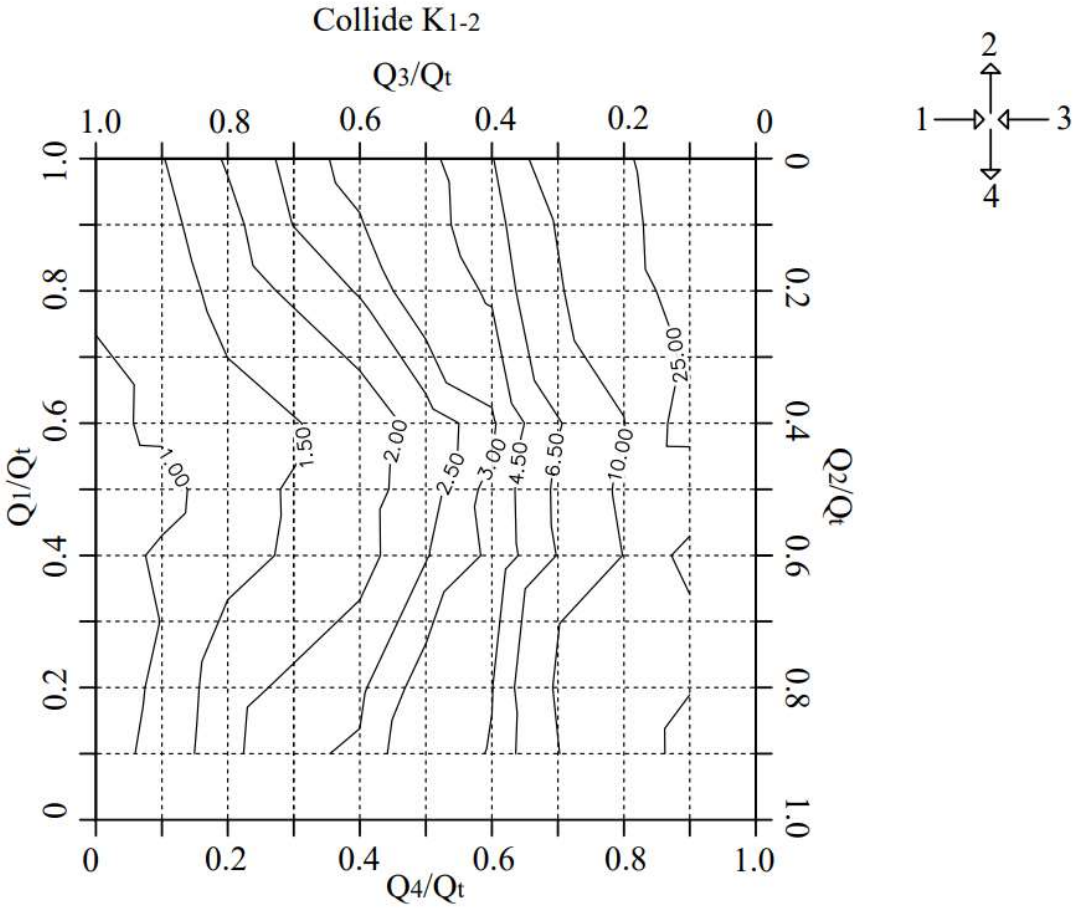

Figure 18. Loss coefficients for Colliding Flow between Leg 1 and 2.

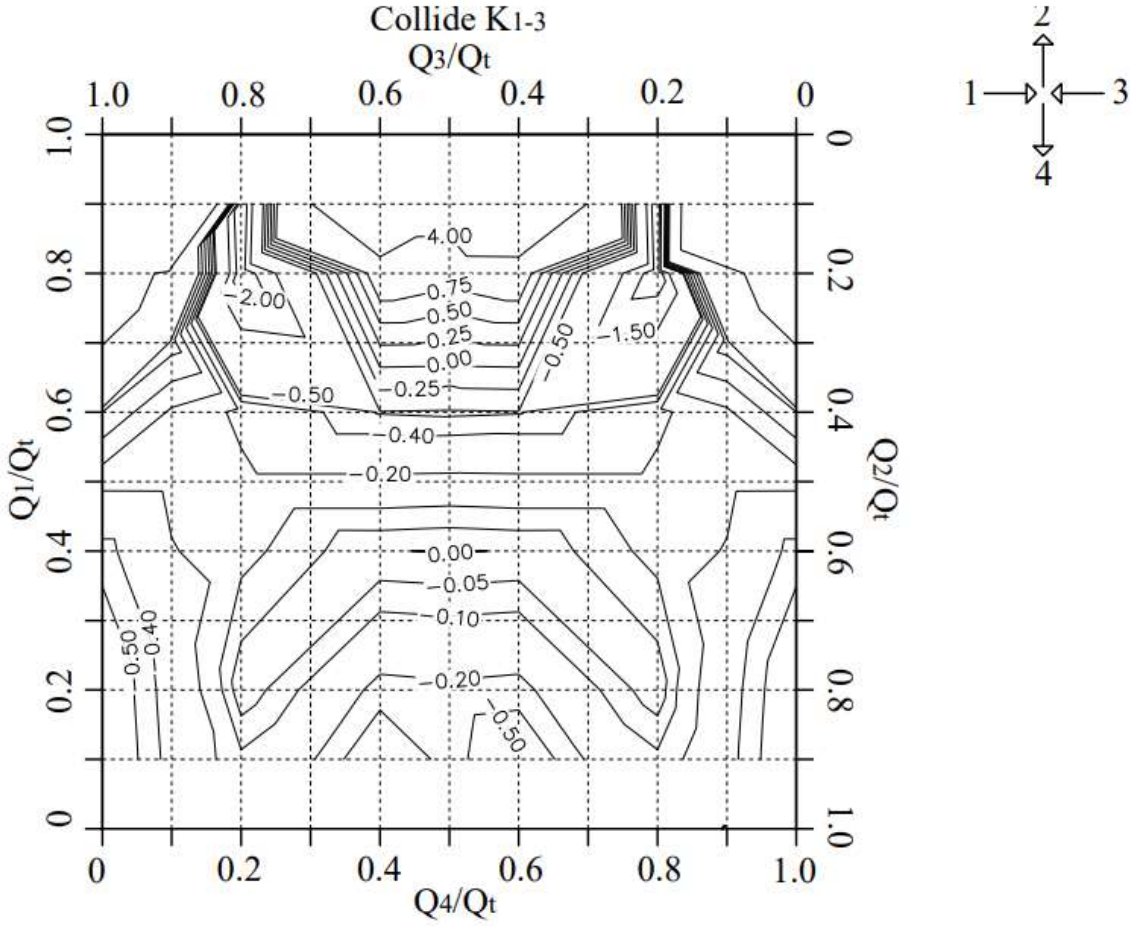

Figure 19. Loss coefficients for Colliding Flow between Leg 1 and 3.

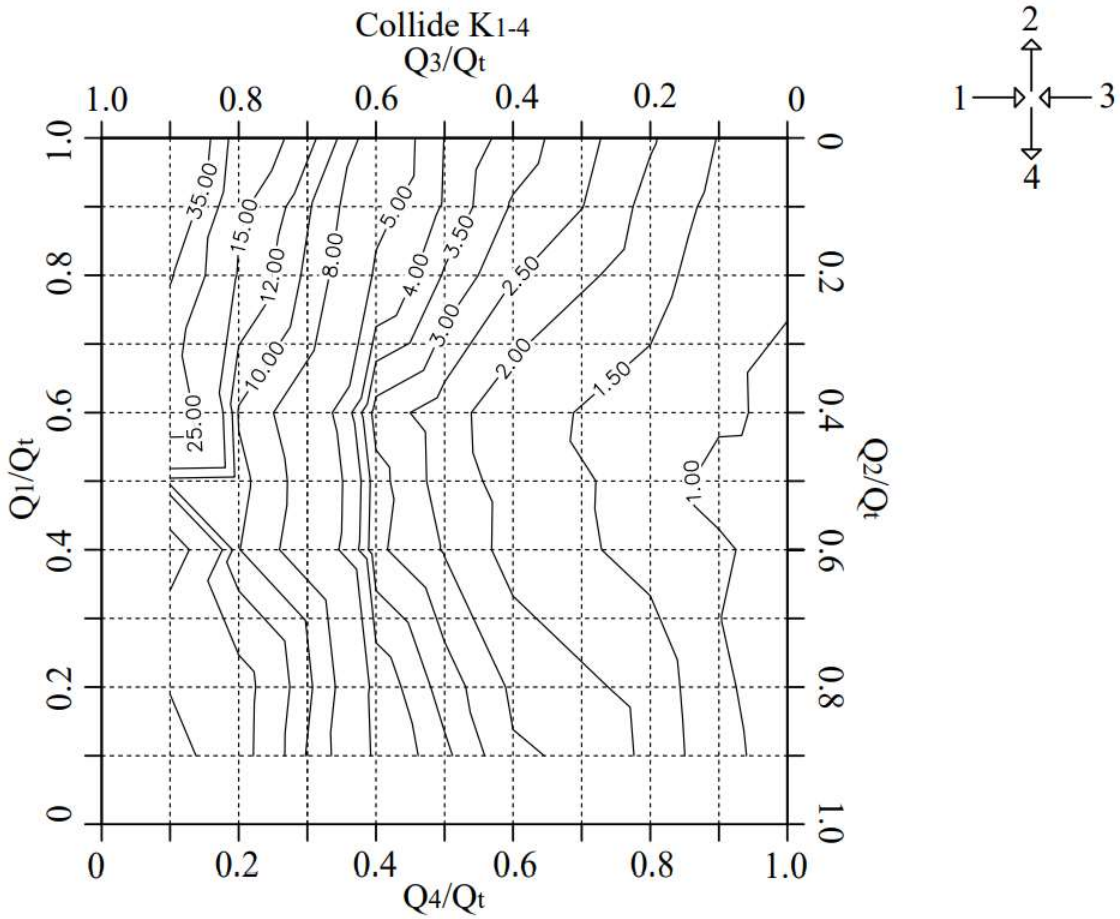

Figure 20. Loss coefficients for Colliding Flow between Leg 1 and 4.

Reynold's Number Independence

The data used to create the contour plots was all for a 6-inch diameter pipe with a square edged cross. To determine whether the 6-inch sharp-edged junction data can be used with other sized pipes, the model was scaled up to have a 24-inch diameter. The 24-inch model was run for a dividing flow with an equal three-way split for two simulations. The first simulation maintained the Reynold's number in each flow leg and the next simulation maintained the same leg velocities as the 6-inch model. The results are shown in Table 4.

Table 4. Data for 6-inch and 24-inch runs.

	Velocity, V (ft/s)				Reynolds Number, Re				Minor Loss Coefficients		
	Leg 1	Leg 2	Leg 3	Leg 4	Leg 1	Leg 2	Leg 3	Leg 4	K_{1-2}	K_{1-3}	K_{1-4}
6 in.	11.89	-3.96	-3.96	-3.96	499266	166425	166413	166433	6.88	-0.43	6.88
24 in.	12.01	-4.00	-4.00	-4.00	1986660	662242	662220	662227	6.96	-0.05	6.96
24 in.	3.02	-1.01	-1.01	-1.01	500297	166771	166766	166768	7.13	-0.05	7.13

The results show small differences in loss coefficient between the 6-inch and 24-inch models in both the equivalent Reynold's number and equivalent velocity situations (Table 5 and 6). The percent difference is large for the K_{1-3} coefficient because the loss coefficient is so small that even slight variations display large changes. For this reason, the magnitude difference is also provided in Tables 4 and 5. The changes between coefficients for runs with equivalent flow ratios are negligible. These data show that the results using the experimental methods outlined are independent of Reynolds number and pipe size.

Table 5. Loss coefficient differences between a 6-inch and 24-inch diameter sharp edged cross (Re = 500,000).

	K_{1-2}	K_{1-3}	K_{1-4}
Magnitude Difference	0.25	0.38	0.25
% Difference	-3.68%	89.14%	-3.67%

Table 6. Loss coefficient differences between a 6-inch and 24-inch diameter sharp edged cross (Inlet Velocity = 12 ft/s).

	K_{1-2}	K_{1-3}	K_{1-4}
Magnitude Difference	0.08	0.38	0.08
% Difference	-1.22%	88.88%	-1.20%

Using the Data

The following example problem will show how a figure is used to determine the losses between leg 1 and legs 2-4 for a dividing flow scenario:

A 6.065-inch diameter four-way junction has an inlet, leg 1, that supplies 1.576 ft^3/s, and splits the flow between the remaining three legs. 30% of the total flow leaves through leg 2, 40% through leg 3, and 30% through leg 4. The pressure in leg is 25 psi, the water temperature is 55 degrees Fahrenheit, and the unit weight of water is 62.39 lb/ft^3. The velocity in leg 1 can be solved with the following equation:

$$V = \frac{Q}{A} \tag{6}$$

Using equation 6, V_1 = 8 ft/s. Because the diameter is in all legs, the split flow ratio can be used to determine the velocity in the remaining legs. V_2 = 8 ft/s · 0.3 = 2.4 ft/s, V_3 = 8 ft/s · 0.4 = 3.2 ft/s, and V_4 = 8 ft/s · 0.3 = 2.4 ft/s.

Using equation 1, head in leg 1 is 58.70 ft. The head in the remaining legs needs to be solved using the K loss coefficients. Equations 1, 2, and 3 were combined to give

the following equation:

$$H_i = H_1 - K\left(\frac{V_i^2}{2g}\right) \tag{7}$$

To determine the head loss coefficients, Figures 9, 10, and 11 are used for $K_{1\text{-}2}$, $K_{1\text{-}3}$, and $K_{1\text{-}4}$, respectively. Figures 21, 22, and 23 show how to use the figures to determine the K factor. From the figures, $K_{1\text{-}2} = 7$, $K_{1\text{-}3} = -0.50$, and $K_{1\text{-}4} = 7$. Using equation 7, $H_2 = 58.07$ ft, $H_3 = 58.78$ ft, $H_4 = 57.07$ ft.

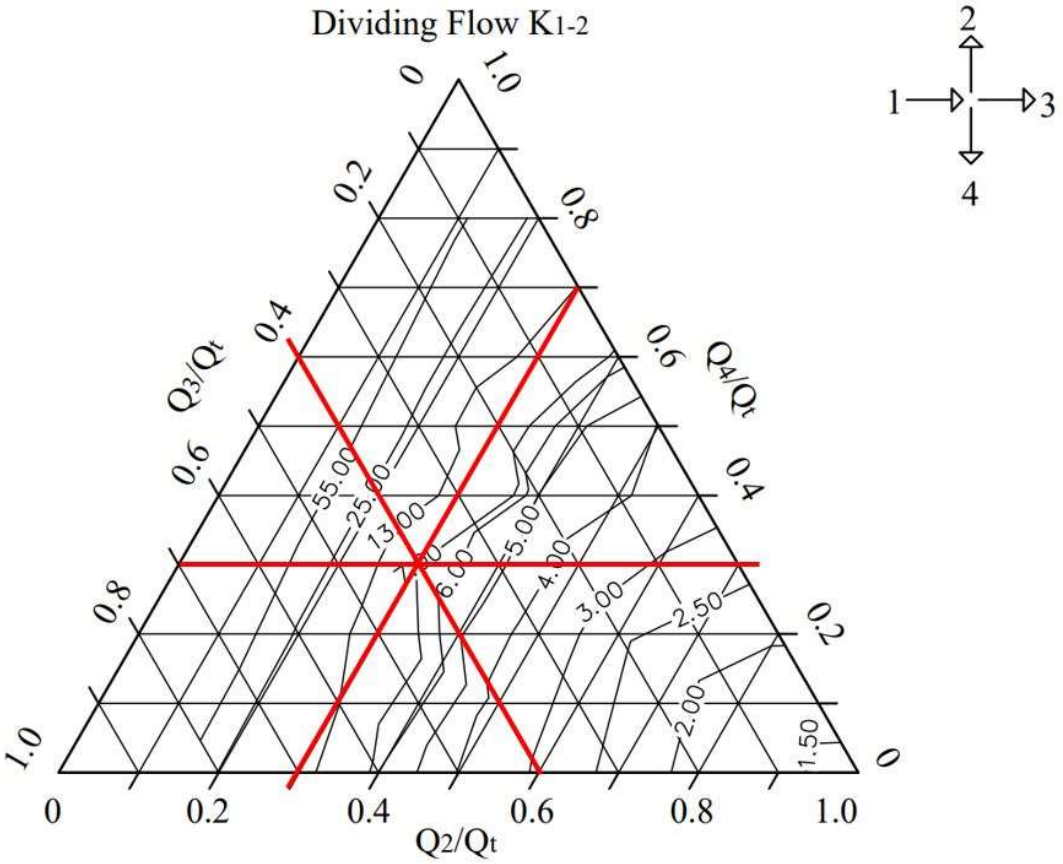

Figure 21. Dividing flow chart showing $K_{1\text{-}2}$ is 7.00.

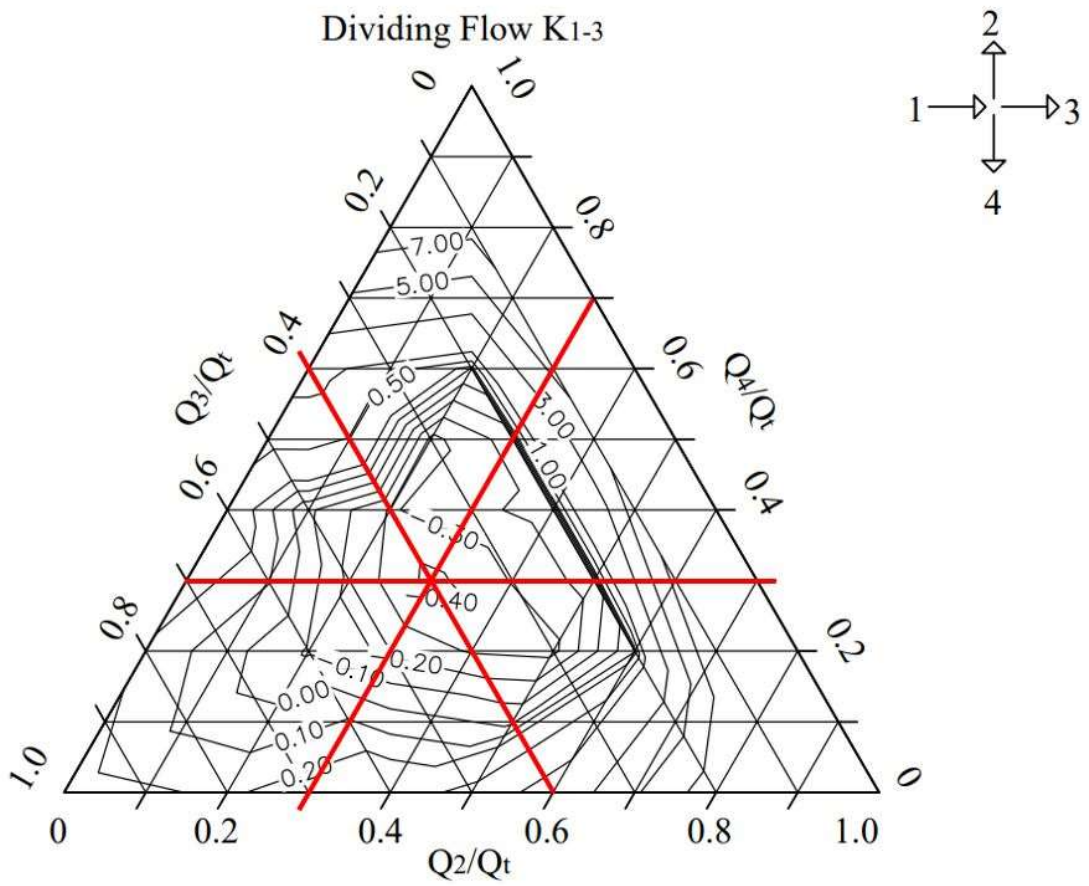

Figure 22. Dividing flow chart showing $K_{1\text{-}3}$ is -0.50.

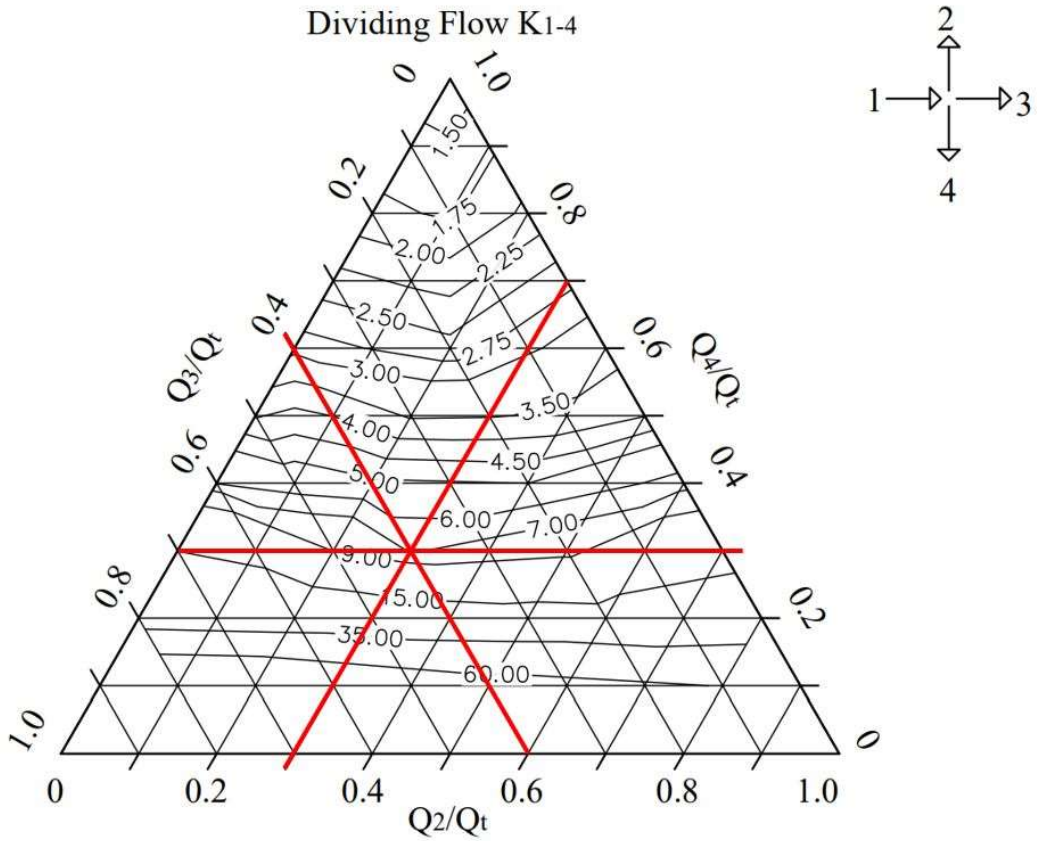

Figure 23. Dividing flow chart showing $K_{1\text{-}4}$ is 7.0.

CHAPTER V

CONCLUSIONS

Research was conducted to determine the best models for determining loss coefficients for four-way cross-junctions using CFD applications. The physics models used were for incompressible, steady-state, turbulent flow, with constant density. The turbulence model used was the Standard k-ε model. The mesh was created using a polyhedral volume mesher, surface remesher, and a prism layer mesher. The results were used to compute loss coefficients which were compared to physical test results to validate the accuracy of the determined models.

The determined models were used to produce additional loss coefficients for sharp-edged crosses. The results were presented in a table, and in twelve contour diagrams for use in pipeline design.

CFD was found to accurately replicate physical data for a round-edged cross. The CFD data was close enough to physical test data to have negligible effects on energy calculations in practical applications.

Additional research to build on this paper could include a more in-depth analysis of the difference in pipe diameter and CFD loss coefficient. Also, losses through different cross types such as junctions of pipes that are not perpendicular, and crosses with different radii.

REFERENCES

Andersson, B., Andersson, R., Hakansson, L., Mortensen, M., Sudiyo, R., & van Wachem, B. (2011). *Computational Fluid Dynamics for Engineers.* Cambridge University Press.

Cebeci, T., Kafyeke, F., & Laurendeau, E. (2005). *Computational Fluid Dynamics for Engineers: From Panel to Navier-Stokes Methods with Computer Programs.* Berlin: Springer.

Celik, I. B., Ghia, U., Roache, P. J., Freitas, C. J., Coleman, H., & Raad, P. E. (2008). Procedure for estimation and reporting of uncertainty due to discretization in CFD applications. *Journal of Fluids Engineering, 130(7)*, 07080011-0780014.

Dent, Patrick, "Develop Design Data on Pressure Loss of Large Pipe Fittings" (2000). *All Graduate Theses and Dissertations*. 7977. https://digitalcommons.usu.edu/etd/7977

Durbin, P., & Petterson Reif, B. (2011). *Statistical Theory and Modeling for Turbulent Flows* (2nd ed.). John Wiley and Sons, Ltd.

Finnemore, E. J., & Franzini, J. B. (2002). *Fluid Mechanics with Engineering Applications* (10th ed.). New York: McGraw Hill.

Jones, W. P., & Launder, B. E. (1973). The Prediction of Laminarization with a Two-Equation Model of Turbulence. *International Journal of Heat Mass Transfer, 5*, 301-314.

Kajishima, T., & Taira, K. (2017). *Computational Fluid Dynamics Incompressible Turbulent Flows.* Springer.

Larsson, S., Lindmark, E. M., Lundstrom, T. S., & Nathan, G. J. (2011). Secondary Flow in Semi-Circular Ducts. *Journal of Fluids Engineering*.

Miller, D. S. (1990). *Internal Flow Systems* (2nd ed.). BHRA.

Moujaes, S., & Deshmukh, S. (2006). Three-Dimensional CFD Predications and Experimental Comparison of Pressure Drop of Some Common Pipe Fittings in Turbulent Flow. *Journal of Energy Engineering*, 61-66.

Nikfetrat, K., Johnson, M. C., & Sharp, Z. B. (2015). Computer Simulations Using Patern Specific Loss Coefficients for Cross Junctions. *Journal of Hydraulic Engineering*.

Oka, K., & Ito, H. (2005). Energy Losses at Tees With Large Area Ratios. *Journal of Fluids Engineering, 127*, 110-116.

Oka, K., Nozaki, T., & Ito, H. (1996). Energy Losses Due to Combination Flow at Tees. *JSME International, 39*(3), 489-498.

Ramamurthy, A. S., Qu, J., & Chao, Z. (2006). 3D Simulation of Combining Flows in 90 degree Rectangular Closed Conduits. *Journal of Hydraulic Engineering*, 214-218.

Rodi, W. (2017). Turbulence Modeling and Simulation in Hydraulics: A Historical Review. *Journal of Hydraulic Engineering, 143*(5).

Sharp, Z. B., Johnson, M. C., Barfuss, S. L., & Rahmeyer, W. J. (2010). Energy Losses in Cross Junctions. *Journal of Hydraulic Engineering*.

Streeter, V. L., & Wylie, E. B. (1975). *Fluid Mechanics* (6th ed.). McGraw-Hill Book Company.

Tullis, J. P. (1989). *Hydraulics of Pipelines; pumps, valves, cavitation, transients.* John Wiley & Sons, Inc.

APPENDIX

APPENDIX

Table A1. Summary of sharp-edged junction loss coefficients for all flow ratios.

Run	Configuration	Flow Split Ratio (+ and – values denote inflow and outflow, respectively)				Flowrate, *Qi* (cfs)				Minor Loss Coefficients, *K*		
		Leg 1	Leg 2	Leg 3	Leg 4	Leg 1	Leg 2	Leg 3	Leg 4	K_{1-2}	K_{1-3}	K_{1-4}
1	Divide	1	-0.2	-0.8	0	2.41	-0.48	-1.93	0.00	23.87	0.18	∞
2	Divide	1	-0.4	-0.6	0	2.41	-0.96	-1.44	0.00	5.97	0.33	∞
3	Divide	1	-0.5	-0.5	0	2.41	-1.20	-1.20	0.00	3.95	0.60	∞
4	Divide	1	-0.6	-0.4	0	2.41	-1.44	-0.96	0.00	2.88	1.28	∞
5	Divide	1	-0.8	-0.2	0	2.41	-1.93	-0.48	0.00	1.82	8.23	∞
6	Divide	1	-0.2	0	-0.8	2.41	-0.48	0.00	-1.93	19.35	∞	2.06
7	Divide	1	-0.4	0	-0.6	2.41	-0.96	0.00	-1.44	6.36	∞	3.28
8	Divide	1	-0.5	0	-0.5	2.41	-1.20	0.00	-1.20	3.98	∞	3.98
9	Divide	1	-0.33	-0.33	-0.33	2.41	-0.80	-0.80	-0.80	6.88	-0.43	6.88
10	Divide	1	-0.3	-0.2	-0.5	2.41	-0.72	-0.48	-1.20	8.17	-0.15	3.46
11	Divide	1	-0.3	-0.5	-0.2	2.41	-0.72	-1.20	-0.48	8.90	-0.23	18.87
12	Divide	1	-0.2	-0.3	-0.5	2.41	-0.48	-0.72	-1.20	17.16	-0.33	3.44
13	Divide	1	-0.4	-0.2	-0.4	2.41	-0.96	-0.48	-0.96	4.99	-0.15	4.99
14	Divide	1	-0.4	-0.4	-0.2	2.41	-0.96	-0.96	-0.48	5.10	-0.31	17.81
15	Divide	1	-0.2	-0.2	-0.6	2.41	-0.48	-0.48	-1.44	16.83	0.09	2.59
16	Divide	1	-0.2	-0.6	-0.2	2.41	-0.48	-1.44	-0.48	20.30	-0.11	20.29
17	Divide	1	-1	0	0	2.41	-2.41	0.00	0.00	1.34	∞	∞
18	Divide	1	0	-1	0	2.41	0.00	-2.41	0.00	∞	0.25	∞
19	Divide	1	0	-0.8	-0.2	2.41	0.00	-1.93	-0.48	∞	0.18	23.87
20	Divide	1	0	-0.6	-0.4	2.41	0.00	-1.44	-0.96	∞	0.33	5.97
21	Divide	1	0	-0.5	-0.5	2.41	0.00	-1.20	-1.20	∞	0.60	3.95
22	Divide	1	0	-0.4	-0.6	2.41	0.00	-0.96	-1.44	∞	1.28	2.88
23	Divide	1	0	-0.2	-0.8	2.41	0.00	-0.48	-1.93	∞	8.23	1.82
24	Divide	1	-0.8	0	-0.2	2.41	-1.93	0.00	-0.48	2.06	∞	19.35
25	Divide	1	-0.6	0	-0.4	2.41	-1.44	0.00	-0.96	3.28	∞	6.36
26	Divide	1	-0.5	-0.2	-0.3	2.41	-1.20	-0.48	-0.72	3.46	-0.15	8.17
27	Divide	1	-0.2	-0.5	-0.3	2.41	-0.48	-1.20	-0.72	18.87	-0.23	8.90
28	Divide	1	-0.5	-0.3	-0.2	2.41	-1.20	-0.72	-0.48	3.44	-0.33	17.16
29	Divide	1	-0.2	-0.4	-0.4	2.41	-0.48	-0.96	-0.96	17.81	-0.31	5.10
30	Divide	1	-0.6	-0.2	-0.2	2.41	-1.44	-0.48	-0.48	2.59	0.09	16.83
31	Divide	1	0	0	-1	2.41	0.00	0.00	-2.41	∞	∞	1.34
32	Divide	1	-0.8	-0.1	-0.1	2.41	-1.93	-0.24	-0.24	1.71	10.75	59.43
33	Divide	1	-0.5	-0.4	-0.1	2.41	-1.20	-0.96	-0.24	3.56	-0.02	68.79

34	Divide	1	-0.1	-0.8	-0.1	2.41	-0.24	-1.93	-0.24	91.40	0.08	91.38
35	Divide	1	-0.1	-0.5	-0.4	2.41	-0.24	-1.20	-0.96	73.45	-0.08	5.41
36	Divide	1	-0.1	-0.1	-0.8	2.41	-0.24	-0.24	-1.93	59.64	7.61	1.71
37	Divide	1	-0.4	-0.1	-0.5	2.41	-0.96	-0.24	-1.20	5.12	4.35	3.58
38	Combine	0.33	0.33	0.33	-1	0.79	0.79	0.79	-2.38	-0.59	-0.18	0.62
39	Combine	0.2	0.5	0.3	-1	0.48	1.20	0.72	-2.41	-1.15	-1.01	0.39
40	Combine	0.3	0.4	0.3	-1	0.72	0.96	0.72	-2.41	-0.82	-0.18	0.56
41	Combine	0.4	0.3	0.3	-1	0.96	0.72	0.72	-2.41	-0.10	0.43	0.68
42	Combine	0.5	0.2	0.3	-1	1.20	0.48	0.72	-2.41	2.11	0.87	0.77
43	Combine	0.5	0.3	0.2	-1	1.20	0.72	0.48	-2.41	0.50	3.94	0.74
44	Combine	0.2	0.4	0.4	-1	0.48	0.96	0.96	-2.41	-1.24	-0.97	0.49
45	Combine	0.2	0.2	0.6	-1	0.48	0.48	1.44	-2.41	-1.32	-0.70	0.64
46	Combine	0.2	0.6	0.2	-1	0.48	1.45	0.48	-2.41	-1.09	-0.19	0.27
47	Combine	0.4	0.2	0.4	-1	0.96	0.48	0.96	-2.41	0.89	-0.17	0.72
48	Combine	0	0.2	0.8	-1	0.00	0.48	1.93	-2.41	∞	∞	∞
49	Combine	0	0.4	0.6	-1	0.00	0.96	1.44	-2.41	∞	∞	∞
50	Combine	0	0.5	0.5	-1	0.00	1.20	1.20	-2.41	∞	∞	∞
51	Combine	0	0.6	0.4	-1	0.00	1.45	0.96	-2.41	∞	∞	∞
52	Combine	0	0.8	0.2	-1	0.00	1.93	0.48	-2.41	∞	∞	∞
53	Combine	0.2	0	0.8	-1	0.48	0.00	1.93	-2.41	∞	-0.64	0.75
54	Combine	0.4	0	0.6	-1	0.96	0.00	1.44	-2.41	∞	-0.45	0.76
55	Combine	0.5	0	0.5	-1	1.20	0.00	1.20	-2.41	∞	-0.16	0.79
56	Combine	0.3	0.5	0.2	-1	0.72	1.20	0.48	-2.41	-0.86	1.68	0.47
57	Combine	0.3	0.3	0.4	-1	0.72	0.72	0.96	-2.41	-0.70	-0.51	0.63
58	Combine	0.3	0.2	0.5	-1	0.72	0.48	1.20	-2.41	-0.24	-0.54	0.68
59	Combine	0.2	0.3	0.5	-1	0.48	0.72	1.20	-2.41	-1.33	-0.82	0.58
60	Combine	0.4	0.4	0.2	-1	0.96	0.96	0.48	-2.41	-0.43	3.04	0.62
61	Combine	0.6	0.2	0.2	-1	1.44	0.48	0.48	-2.41	3.58	4.72	0.84
62	Combine	0.8	0.2	0	-1	1.93	0.48	0.00	-2.41	7.46	∞	1.02
63	Combine	0.6	0.4	0	-1	1.44	0.96	0.00	-2.41	0.34	∞	0.76
64	Combine	0.5	0.5	0	-1	1.20	1.20	0.00	-2.41	-0.31	∞	0.62
65	Combine	0.4	0.6	0	-1	0.96	1.45	0.00	-2.41	-0.65	∞	0.44
66	Combine	0.2	0.8	0	-1	0.48	1.93	0.00	-2.41	-0.99	∞	-0.05
67	Combine	0.8	0	0.2	-1	1.93	0.00	0.48	-2.41	∞	7.77	1.07
68	Combine	0.6	0	0.4	-1	1.44	0.00	0.96	-2.41	∞	0.50	0.86
69	Combine	0	1	0	-1	0.00	2.41	0.00	-2.41	∞	∞	∞
70	Combine	1	0	0	-1	2.41	0.00	0.00	-2.41	∞	∞	1.34
71	Combine	0	0	1	-1	0.00	0.00	2.41	-2.41	∞	∞	∞
72	Combine	0.1	0.1	0.8	-1	0.24	0.24	1.93	-2.41	-1.86	-0.69	0.69
73	Combine	0.1	0.8	0.1	-1	0.24	1.93	0.24	-2.41	-1.16	-0.22	-0.18
74	Combine	0.8	0.1	0.1	-1	1.93	0.24	0.24	-2.41	32.66	34.31	1.04

75	Combine	0.5	0.4	0.1	-1	1.20	0.96	0.24	-2.41	-0.06	25.53	0.69
76	Combine	0.4	0.5	0.1	-1	0.96	1.20	0.24	-2.41	-0.58	22.05	0.54
77	Combine	0.1	0.4	0.5	-1	0.24	0.96	1.20	-2.41	-1.66	-1.19	0.43
78	Perp	0.8	0.2	0	-1	1.93	0.48	0.00	-2.41	7.44	∞	1.02
79	Perp	0.8	0.2	-0.2	-0.8	1.93	0.48	-0.48	-1.93	7.98	9.98	1.35
80	Perp	0.8	0.2	-0.4	-0.6	1.93	0.48	-0.96	-1.44	8.78	2.26	2.11
81	Perp	0.8	0.2	-0.5	-0.5	1.93	0.48	-1.20	-1.20	9.31	1.42	2.91
82	Perp	0.8	0.2	-0.6	-0.4	1.93	0.48	-1.44	-0.96	9.92	0.99	4.41
83	Perp	0.8	0.2	-0.8	-0.2	1.93	0.48	-1.93	-0.48	11.44	0.60	17.48
84	Perp	0.6	0.4	-0.8	-0.2	1.44	0.96	-1.93	-0.48	0.73	0.78	11.79
85	Perp	0.6	0.4	-0.6	-0.4	1.44	0.96	-1.44	-0.96	0.58	1.19	3.04
86	Perp	0.6	0.4	-0.5	-0.5	1.44	0.96	-1.20	-1.20	0.52	1.64	2.03
87	Perp	0.6	0.4	-0.4	-0.6	1.44	0.96	-0.96	-1.44	0.48	2.47	1.50
88	Perp	0.6	0.4	-0.2	-0.8	1.44	0.96	-0.48	-1.93	0.41	9.27	0.99
89	Perp	0.6	0.4	0	-1	1.44	0.96	0.00	-2.41	0.34	∞	0.76
90	Perp	0.6	0.4	-1	0	1.44	0.96	-2.41	0.00	0.93	0.62	∞
91	Perp	0.5	0.5	0	-1	1.20	1.20	0.00	-2.41	-0.31	∞	0.62
92	Perp	0.5	0.5	-0.2	-0.8	1.20	1.20	-0.48	-1.93	-0.24	8.85	0.80
93	Perp	0.5	0.5	-0.5	-0.5	1.20	1.20	-1.20	-1.20	-0.16	1.64	1.64
94	Perp	0.5	0.5	-0.6	-0.4	1.20	1.20	-1.44	-0.96	-0.14	1.22	2.43
95	Perp	0.6	0.4	-1	0	1.44	0.96	-2.41	0.00	0.93	0.62	∞
96	Perp	0.8	0.2	-1	0	1.93	0.48	-2.41	0.00	13.28	0.49	∞
97	Perp	1	0	0	-1	2.41	0.00	0.00	-2.41	∞	∞	1.34
98	Perp	1	0	-1	0	2.41	0.00	-2.41	0.00	∞	0.25	∞
99	Perp	0	1	-1	0	0.00	2.41	-2.41	0.00	∞	∞	∞
100	Perp	0	1	0	-1	0.00	2.41	0.00	-2.41	∞	∞	∞
101	Perp	1	0	-0.2	-0.8	2.41	0.00	-0.48	-1.93	∞	8.23	1.82
102	Perp	1	0	-0.4	-0.6	2.41	0.00	-0.96	-1.44	∞	1.28	2.88
103	Perp	1	0	-0.5	-0.5	2.41	0.00	-1.20	-1.20	∞	0.60	3.95
104	Perp	1	0	-0.6	-0.4	2.41	0.00	-1.44	-0.96	∞	0.33	5.97
105	Perp	1	0	-0.8	-0.2	2.41	0.00	-1.93	-0.48	∞	0.18	23.87
106	Perp	0	1	-0.2	-0.8	0.00	2.41	-0.48	-1.93	∞	∞	∞
107	Perp	0	1	-0.4	-0.6	0.00	2.41	-0.96	-1.44	∞	∞	∞
108	Perp	0	1	-0.6	-0.4	0.00	2.41	-1.44	-0.96	∞	∞	∞
109	Perp	0	1	-0.8	-0.2	0.00	2.41	-1.93	-0.48	∞	∞	∞
110	Perp	0.2	0.8	-1	0	0.48	1.93	-2.41	0.00	-0.62	0.72	∞
111	Perp	0.2	0.8	-0.8	-0.2	0.48	1.93	-1.93	-0.48	-0.66	0.83	1.79
112	Perp	0.2	0.8	-0.6	-0.4	0.48	1.93	-1.44	-0.96	-0.71	1.12	0.02
113	Perp	0.2	0.8	-0.5	-0.5	0.48	1.93	-1.20	-1.20	-0.74	1.39	-0.10
114	Perp	0.2	0.8	-0.4	-0.6	0.48	1.93	-0.96	-1.44	-0.78	1.88	-0.14
115	Perp	0.2	0.8	-0.2	-0.8	0.48	1.93	-0.48	-1.93	-0.87	5.83	-0.12

116	Perp	0.4	0.6	-0.2	-0.8	0.96	1.44	-0.48	-1.93	-0.55	8.21	0.56
117	Perp	0.4	0.6	-0.4	-0.6	0.96	1.44	-0.96	-1.44	-0.49	2.29	0.86
118	Perp	0.4	0.6	-0.5	-0.5	0.96	1.44	-1.20	-1.20	-0.46	1.58	1.19
119	Perp	0.4	0.6	-0.6	-0.4	0.96	1.44	-1.44	-0.96	-0.44	1.21	1.82
120	Perp	0.4	0.6	-0.8	-0.2	0.96	1.44	-1.93	-0.48	-0.41	0.85	6.98
121	Perp	0.4	0.6	-1	0	0.96	1.44	-2.41	0.00	-0.38	0.68	∞
122	Perp	0.4	0.6	0	-1	0.96	1.44	0.00	-2.41	-0.65	∞	0.45
123	Perp	0.5	0.5	-1	0	1.20	1.20	-2.41	0.00	-0.01	0.66	∞
124	Perp	0.5	0.5	-0.8	-0.2	1.20	1.20	-1.93	-0.48	-0.08	0.83	9.33
125	Perp	0.5	0.5	-0.4	-0.6	1.20	1.20	-0.96	-1.44	-0.18	2.40	1.21
126	Perp	0.2	0.8	0	-1	0.48	1.93	0.00	-2.41	-0.99	∞	-0.05
127	Perp	0.9	0.1	-1	0	2.17	0.24	-2.41	0.00	76.21	0.38	∞
128	Perp	0.9	0.1	-0.9	-0.1	2.17	0.24	-2.17	-0.24	71.01	0.38	85.46
129	Perp	0.9	0.1	-0.8	-0.2	2.17	0.24	-1.93	-0.48	66.12	0.44	20.66
130	Perp	0.9	0.1	-0.7	-0.3	2.17	0.24	-1.68	-0.72	61.67	0.55	9.15
131	Perp	0.9	0.1	-0.6	-0.4	2.17	0.24	-1.44	-0.96	57.59	0.76	5.20
132	Perp	0.9	0.1	-0.5	-0.5	2.17	0.24	-1.20	-1.20	54.05	1.15	3.42
133	Perp	0.9	0.1	-0.4	-0.6	2.17	0.24	-0.96	-1.44	50.99	1.92	2.48
134	Perp	0.9	0.1	-0.3	-0.7	2.17	0.24	-0.72	-1.68	48.41	3.76	1.93
135	Perp	0.9	0.1	-0.2	-0.8	2.17	0.24	-0.48	-1.93	46.23	9.42	1.57
136	Perp	0.9	0.1	-0.1	-0.9	2.17	0.24	-0.24	-2.17	44.47	42.04	1.33
137	Perp	0.9	0.1	0	-1	2.17	0.24	0.00	-2.41	43.08	∞	1.17
138	Perp	1	0	-0.9	-0.1	2.41	0.00	-2.17	-0.24	∞	0.19	98.31
139	Perp	0.8	0.2	-0.9	-0.1	1.93	0.48	-2.17	-0.24	12.33	0.52	72.27
140	Perp	0.7	0.3	-0.9	-0.1	1.68	0.72	-2.17	-0.24	3.35	0.62	59.88
141	Perp	0.6	0.4	-0.9	-0.1	1.44	0.96	-2.17	-0.24	0.83	0.68	48.43
142	Perp	0.5	0.5	-0.9	-0.1	1.20	1.20	-2.17	-0.24	-0.06	0.72	37.97
143	Perp	0.4	0.6	-0.9	-0.1	0.96	1.45	-2.17	-0.24	-0.40	0.75	28.35
144	Perp	0.3	0.7	-0.9	-0.1	0.72	1.69	-2.17	-0.24	-0.56	0.77	19.01
145	Perp	0.2	0.8	-0.9	-0.1	0.48	1.93	-2.17	-0.24	-0.64	0.76	9.59
146	Perp	0	1	-0.9	-0.1	0.00	2.41	-2.17	-0.24	∞	∞	∞
147	Perp	0.1	0.9	0	-1	0.24	2.17	0.00	-2.41	-1.09	∞	-0.39
148	Perp	0.1	0.9	-0.1	-0.9	0.24	2.17	-0.24	-2.17	-1.02	14.11	-0.50
149	Perp	0.1	0.9	-0.2	-0.8	0.24	2.17	-0.48	-1.93	-0.96	4.04	-0.60
150	Perp	0.1	0.9	-0.3	-0.7	0.24	2.17	-0.72	-1.68	-0.91	2.26	-0.71
151	Perp	0.1	0.9	-0.4	-0.6	0.24	2.17	-0.96	-1.44	-0.86	1.58	-0.85
152	Perp	0.1	0.9	-0.5	-0.5	0.24	2.17	-1.20	-1.20	-0.81	1.25	-1.03
153	Perp	0.1	0.9	-0.6	-0.4	0.24	2.17	-1.44	-0.96	-0.78	1.06	-1.29
154	Perp	0.1	0.9	-0.7	-0.3	0.24	2.17	-1.68	-0.72	-0.74	0.93	-1.66
155	Perp	0.1	0.9	-0.8	-0.2	0.24	2.17	-1.93	-0.48	-0.72	0.84	-2.21
156	Perp	0.1	0.9	-0.9	-0.1	0.24	2.17	-2.17	-0.24	-0.70	0.78	-2.72

157	Perp	0.1	0.9	-1	0	0.24	2.17	-2.41	0.00	-0.68	0.74	∞
158	Perp	0	1	-0.1	-0.9	0.00	2.41	-0.24	-2.17	∞	∞	∞
159	Perp	0.2	0.8	-0.1	-0.9	0.48	1.93	-0.24	-2.17	-0.93	22.08	-0.10
160	Perp	0.3	0.7	-0.1	-0.9	0.72	1.68	-0.24	-2.17	-0.80	28.10	0.22
161	Perp	0.4	0.6	-0.1	-0.9	0.96	1.44	-0.24	-2.17	-0.60	32.51	0.48
162	Perp	0.5	0.5	-0.1	-0.9	1.20	1.20	-0.24	-2.17	-0.26	35.38	0.69
163	Perp	0.6	0.4	-0.1	-0.9	1.45	0.96	-0.24	-2.17	0.39	37.23	0.86
164	Perp	0.7	0.3	-0.1	-0.9	1.69	0.72	-0.24	-2.17	2.04	38.93	1.01
165	Perp	0.8	0.2	-0.1	-0.9	1.93	0.48	-0.24	-2.17	7.75	41.34	1.16
166	Perp	1	0	-0.1	-0.9	2.41	0.00	-0.24	-2.17	∞	39.68	1.54
167	Collide	0.8	-0.8	0.2	-0.2	1.93	-1.93	0.48	-0.48	1.68	-2.35	14.35
168	Collide	0.8	-0.6	0.2	-0.4	1.93	-1.44	0.48	-0.96	2.55	1.06	4.74
169	Collide	0.8	-0.5	0.2	-0.5	1.93	-1.20	0.48	-1.20	3.44	0.90	3.44
170	Collide	0.8	-1	0.2	0	1.93	-2.41	0.48	0.00	1.07	7.74	∞
171	Collide	0.6	-0.5	0.4	-0.5	1.44	-1.20	0.96	-1.20	2.23	-0.52	2.23
172	Collide	0.6	-0.6	0.4	-0.4	1.44	-1.44	0.96	-0.96	1.64	-0.51	2.77
173	Collide	0.6	-0.8	0.4	-0.2	1.44	-1.93	0.96	-0.48	1.32	-0.24	9.77
174	Collide	0.6	-1	0.4	0	1.44	-2.41	0.96	0.00	0.86	0.50	∞
175	Collide	0.5	-0.8	0.5	-0.2	1.20	-1.93	1.20	-0.48	1.30	-0.16	10.65
176	Collide	0.5	-0.6	0.5	-0.4	1.20	-1.44	1.20	-0.96	1.80	-0.16	3.19
177	Collide	0.5	-0.5	0.5	-0.5	1.20	-1.20	1.20	-1.20	2.26	-0.16	2.25
178	Collide	0.5	-1	0.5	0	1.20	-2.41	1.20	0.00	0.79	-0.16	∞
179	Collide	0.2	-0.8	0.8	-0.2	0.48	-1.93	1.93	-0.48	1.82	-0.01	16.50
180	Collide	0.2	-0.6	0.8	-0.4	0.48	-1.44	1.93	-0.96	2.41	-0.22	4.43
181	Collide	0.2	-0.5	0.8	-0.5	0.48	-1.20	1.93	-1.20	3.27	-0.21	3.27
182	Collide	0.2	-1	0.8	0	0.48	-2.41	1.93	0.00	0.75	-0.64	∞
183	Collide	0.4	-0.5	0.6	-0.5	0.96	-1.20	1.44	-1.20	2.46	0.00	2.46
184	Collide	0.4	-0.6	0.6	-0.4	0.96	-1.44	1.44	-0.96	1.79	0.00	3.11
185	Collide	0.4	-0.8	0.6	-0.2	0.96	-1.93	1.44	-0.48	1.34	-0.12	10.07
186	Collide	0.4	-1	0.6	0	0.96	-2.41	1.44	0.00	0.76	-0.45	∞
187	Collide	0.8	-0.2	0.2	-0.8	1.93	-0.48	0.48	-1.93	14.35	-2.35	1.68
188	Collide	0.8	-0.4	0.2	-0.6	1.93	-0.96	0.48	-1.44	4.74	1.06	2.55
189	Collide	0.8	0	0.2	-1	1.93	0.00	0.48	-2.41	∞	7.74	1.07
190	Collide	0.6	-0.4	0.4	-0.6	1.44	-0.96	0.96	-1.44	2.77	-0.51	1.64
191	Collide	0.6	-0.2	0.4	-0.8	1.44	-0.48	0.96	-1.93	9.77	-0.24	1.32
192	Collide	0.6	0	0.4	-1	1.44	0.00	0.96	-2.41	∞	0.50	0.86
193	Collide	0.5	-0.2	0.5	-0.8	1.20	-0.48	1.20	-1.93	10.65	-0.16	1.30
194	Collide	0.5	-0.4	0.5	-0.6	1.20	-0.96	1.20	-1.44	3.19	-0.16	1.80
195	Collide	0.5	0	0.5	-1	1.20	0.00	1.20	-2.41	∞	-0.16	0.79
196	Collide	0.2	-0.2	0.8	-0.8	0.48	-0.48	1.93	-1.93	16.50	-0.01	1.82
197	Collide	0.2	-0.4	0.8	-0.6	0.48	-0.96	1.93	-1.44	4.43	-0.22	2.41

198	Collide	0.2	0	0.8	-1	0.48	0.00	1.93	-2.41	∞	-0.64	0.75
199	Collide	0.4	-0.4	0.6	-0.6	0.96	-0.96	1.44	-1.44	3.11	0.00	1.79
200	Collide	0.4	-0.2	0.6	-0.8	0.96	-0.48	1.44	-1.93	10.07	-0.12	1.34
201	Collide	0.4	0	0.6	-1	0.96	0.00	1.44	-2.41	∞	-0.45	0.76
202	Collide	1	-1	0	0	2.41	-2.41	0.00	0.00	1.34	∞	∞
203	Collide	1	-0.8	0	-0.2	2.41	-1.93	0.00	-0.48	2.06	∞	19.35
204	Collide	1	-0.6	0	-0.4	2.41	-1.44	0.00	-0.96	3.28	∞	6.36
205	Collide	1	-0.5	0	-0.5	2.41	-1.20	0.00	-1.20	3.98	∞	3.98
206	Collide	1	-0.4	0	-0.6	2.41	-0.96	0.00	-1.44	6.36	∞	3.28
207	Collide	1	-0.2	0	-0.8	2.41	-0.48	0.00	-1.93	19.35	∞	2.06
208	Collide	0	-1	1	0	0.00	-2.41	2.41	0.00	∞	∞	∞
209	Collide	0	-0.8	1	-0.2	0.00	-1.93	2.41	-0.48	∞	∞	∞
210	Collide	0	-0.6	1	-0.4	0.00	-1.44	2.41	-0.96	∞	∞	∞
211	Collide	0	-0.2	1	-0.8	0.00	-0.48	2.41	-1.93	∞	∞	∞
212	Collide	0	-0.4	1	-0.6	0.00	-0.96	2.41	-1.44	∞	∞	∞
213	Collide	0	-0.5	1	-0.5	0.00	-1.20	2.41	-1.20	∞	∞	∞
214	Collide	0	0	1	-1	0.00	0.00	2.41	-2.41	∞	∞	∞
215	Collide	1	0	0	-1	2.41	0.00	0.00	-2.41	∞	∞	1.34
216	Collide	0.9	0	0.1	-1	2.17	0.00	0.24	-2.41	∞	41.64	1.21
217	Collide	0.9	-0.1	0.1	-0.9	2.17	-0.24	0.24	-2.17	46.98	16.53	1.35
218	Collide	0.9	-0.8	0.1	-0.2	2.17	-1.93	0.24	-0.48	1.83	-2.52	15.82
219	Collide	0.9	-0.3	0.1	-0.7	2.17	-0.72	0.24	-1.68	10.28	3.82	2.51
220	Collide	0.9	-0.4	0.1	-0.6	2.17	-0.96	0.24	-1.44	5.46	13.47	2.94
221	Collide	0.9	-0.5	0.1	-0.5	2.17	-1.20	0.24	-1.20	3.90	6.64	3.90
222	Collide	1	-0.9	0	-0.1	2.41	-2.17	0.00	-0.24	1.48	∞	57.59
223	Collide	0.8	-0.9	0.2	-0.1	1.93	-2.17	0.48	-0.24	1.23	2.74	36.14
224	Collide	0.7	-0.9	0.3	-0.1	1.68	-2.17	0.72	-0.24	1.10	0.62	28.15
225	Collide	0.6	-0.9	0.4	-0.1	1.44	-2.17	0.96	-0.24	1.11	-0.05	32.76
226	Collide	0.5	-0.9	0.5	-0.1	1.20	-2.17	1.20	-0.24	0.81	-0.16	11.02
227	Collide	0.1	0	0.9	-1	0.24	0.00	2.17	-2.41	∞	-0.66	0.79
228	Collide	0.1	-0.1	0.9	-0.9	0.24	-0.24	2.17	-2.17	30.21	-0.35	1.14
229	Collide	0.1	-0.8	0.9	-0.2	0.24	-1.93	2.17	-0.48	1.86	-0.11	16.39
230	Collide	0.1	-0.3	0.9	-0.7	0.24	-0.72	2.17	-1.68	9.83	-0.19	2.43
231	Collide	0.1	-0.4	0.9	-0.6	0.24	-0.96	2.17	-1.44	4.61	-0.31	2.56
232	Collide	0.1	-0.5	0.9	-0.5	0.24	-1.20	2.17	-1.20	3.62	-0.23	3.62
233	Collide	0	-0.9	1	-0.1	0.00	-2.17	2.41	-0.24	∞	∞	∞
234	Collide	0.2	-0.9	0.8	-0.1	0.48	-2.17	1.93	-0.24	1.08	-0.33	24.38
235	Collide	0.3	-0.9	0.7	-0.1	0.72	-2.17	1.68	-0.24	1.01	-0.30	20.97
236	Collide	0.4	-0.9	0.6	-0.1	0.96	-2.17	1.44	-0.24	1.08	-0.21	30.79
237	Collide	0.9	-1	0.1	0	2.17	-2.41	0.24	0.00	1.21	41.64	∞
238	Collide	0.9	-0.9	0.1	-0.1	2.17	-2.17	0.24	-0.24	1.35	16.53	46.98

239	Collide	0.9	-0.2	0.1	-0.8	2.17	-0.48	0.24	-1.93	15.82	-2.52	1.83
240	Collide	0.9	-0.7	0.1	-0.3	2.17	-1.68	0.24	-0.72	2.51	3.82	10.28
241	Collide	0.9	-0.6	0.1	-0.4	2.17	-1.44	0.24	-0.96	2.94	13.47	5.46
242	Collide	0.9	-0.5	0.1	-0.5	2.17	-1.20	0.24	-1.20	3.90	6.64	3.90
243	Collide	1	-0.1	0	-0.9	2.41	-0.24	0.00	-2.17	57.59	∞	1.48
244	Collide	0.8	-0.1	0.2	-0.9	1.93	-0.24	0.48	-2.17	36.14	2.74	1.23
245	Collide	0.7	-0.1	0.3	-0.9	1.68	-0.24	0.72	-2.17	28.15	0.62	1.10
246	Collide	0.6	-0.1	0.4	-0.9	1.44	-0.24	0.96	-2.17	32.76	-0.05	1.11
247	Collide	0.5	-0.1	0.5	-0.9	1.20	-0.24	1.20	-2.17	11.02	-0.16	0.81
248	Collide	0.1	-1	0.9	0	0.24	-2.41	2.17	0.00	0.79	-0.66	∞
249	Collide	0.1	-0.9	0.9	-0.1	0.24	-2.17	2.17	-0.24	1.14	-0.35	30.21
250	Collide	0.1	-0.2	0.9	-0.8	0.24	-0.48	2.17	-1.93	16.39	-0.11	1.86
251	Collide	0.1	-0.7	0.9	-0.3	0.24	-1.68	2.17	-0.72	2.43	-0.19	9.83
252	Collide	0.1	-0.6	0.9	-0.4	0.24	-1.44	2.17	-0.96	2.56	-0.31	4.61
253	Collide	0	-0.1	1	-0.9	0.00	-0.24	2.41	-2.17	∞	∞	∞
254	Collide	0.2	-0.1	0.8	-0.9	0.48	-0.24	1.93	-2.17	24.38	-0.33	1.08
255	Collide	0.3	-0.1	0.7	-0.9	0.72	-0.24	1.68	-2.17	20.97	-0.30	1.01
256	Collide	0.4	-0.1	0.6	-0.9	0.96	-0.24	1.44	-2.17	30.79	-0.21	1.08